The stomatal traits that conserve water without compromising grapevine carbon gain depend on climate change severity and wine-growing region

Rami Albasha, Megan K Bartlett

Agricultural and Forest Meteorology 347 (2024) 109892

Contents lists available at ScienceDirect

Agricultural and Forest Meteorology

journal homepage: www.elsevier.com/locate/agrformet

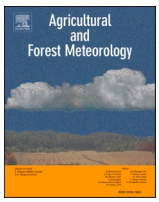

The stomatal traits that conserve water without compromising grapevine carbon gain depend on climate change severity and wine-growing region

Rami Albasha [a,b], Megan K. Bartlett [c,*]

[a] itk society, Clapiers, France
[b] INRAE, UMR759 LEPSE, Montpellier, France
[c] Department of Viticulture and Enology, University of California, Davis, USA

ARTICLE INFO

Keywords:
Stomata
Climate change
Water-use efficiency
Viticulture
Grapes

ABSTRACT

Winegrapes are a valuable ($70 billion) commodity, but climate change is predicted to reduce grape yield and quality by exacerbating water and heat stress. Developing stress-resistant varieties would mitigate these impacts, but the trait values to target can be obscured by complex relationships between traits and plant performance. Stomatal traits mediate trade-offs between increasing gas exchange, to increase carbon assimilation and evaporative cooling, and reducing gas exchange, to avoid water stress. We used a functional-structural plant model to quantify the impacts of maximum stomatal conductance (g_{max}) and leaf water potential thresholds for 50 % stomatal closure (g_s Ψ_{50}) on vine carbon gain, water stress, and temperature under historical and future conditions, assuming moderate and extreme climate change (Representative Concentration Pathways 4.5 and 8.5), for premium- and hot-climate US wine regions (Napa and the San Joaquin Valley (SJV)). Shifting from the mean trait values reported for winegrapes to water-saving values (i.e., a lower g_{max} and less negative g_s Ψ_{50}) reduced simulated vine transpiration and water stress below even historical levels, but the trait values that conserved water without compromising carbon gain varied between climate scenarios and regions. Extreme water-saving traits maintained carbon gain at or above historical levels in Napa under both scenarios, while intermediate water-saving traits maintained carbon gain under moderate climate change in the SJV. Vine canopy temperatures exceeded thresholds for photochemical heat damage in the SJV, regardless of the trait values. Overall, by reducing transpiration and water stress, water-saving traits would reduce irrigation demand and warming impacts on yield and quality, though more work is needed to determine whether historical carbon gain will remain adequate to support ripening, especially with heat-reducing management practices. Developing varieties with a range of water-saving trait values would provide plant material tailored to different regions and reduce the risk from uncertainty around future climate.

1. Introduction

Winegrapes (*Vitis vinifera* L.) are an important crop economically, valued at nearly $70 billion globally, and culturally, evoking a sense of place, time, and community in a way that is unique among commodities (Alston and Sambucci, 2019). Climate change is expected to increase temperature and evaporative demand in many wine-growing regions worldwide (Jones, 2008; White et al., 2006), potentially decreasing yields and reducing wine quality (Jones et al., 2005; Pathak et al., 2018). Developing more stress-resistant crop varieties is a key strategy to adapt agriculture to climate change (Atlin et al., 2017; Duchene, 2016; Vivin et al., 2017). However, few traits have simple, monotonic relationships with plant performance (Messina et al., 2011). Instead, relationships between traits and performance often reflect compromises between competing physiological demands, which obscures the trait values that breeding or genetic engineering should aim to achieve (Chaves et al., 2016; Walker et al., 2018).

Stomatal traits mediate several trade-offs that are important to vine responses to climate change (Chaves et al., 2016). High stomatal conductance increases both transpiration and the CO_2 influx for photosynthesis. A high transpiration rate can exacerbate plant water stress by dehydrating the leaves and depleting soil moisture, but also mitigate heat stress by increasing the evaporative cooling of the foliage (Drake et al., 2018; Wolf et al., 2016). High leaf temperatures can

* Corresponding author.
E-mail address: mkbartlett@ucdavis.edu (M.K. Bartlett).

https://doi.org/10.1016/j.agrformet.2024.109892
Received 20 October 2023; Received in revised form 5 January 2024; Accepted 7 January 2024
Available online 22 January 2024

damage the biochemical machinery for photosynthesis and cause lasting reductions in carbon gain (Greer and Weedon, 2013; Hüve et al., 2011). Thus, under hot conditions, with a high evaporative demand, plants face a trade-off between closing the stomata to avoid water stress, and keeping the stomata open to maintain photosynthesis and evaporative cooling.

Stomatal behavior can also affect grape yield and berry chemistry. Water stress can reduce yield by limiting the water supply for berry growth, or inducing wilting or leaf senescence that overexposes and sunburns the fruit (Coombe and McCarthy, 2000; Keller et al., 2015; Webb et al., 2010). High-quality berries have an appropriate ratio of sugar to acid content and, for red varieties, a high anthocyanin content. Insufficient photosynthesis can prevent berries from reaching adequate sugar levels for winemaking, while water stress can overly concentrate sugars and accelerate the degradation of acids and anthocyanins through overexposure (Alston et al., 2018; Jones et al., 2005; Martínez-Lüscher et al., 2020). Altogether, improved grape cultivars need stomatal traits that balance competing demands for carbon gain, avoiding water stress, and evaporative cooling under future climatic conditions.

Several findings suggest that growers would benefit most from stomatal traits that reduce gas exchange to prioritize avoiding vine water stress and reducing irrigation demand. Modeling and experimental work in agronomic crops (e.g., chickpeas, wheat, and soybeans) found that cultivars with lower maximum gas exchange rates conserved soil moisture longer into the growing season, which reduced differences in yield between well-watered and non-irrigated conditions (Sinclair et al., 2010, 2005; Zaman-Allah et al., 2011). Consistent with these findings, a meta-analysis of grape physiology traits found that maximum stomatal conductance was lower in cultivars that produce high-quality wine in hotter, drier regions (Bartlett and Sinclair, 2021). Further, recent modeling work found that stomatal traits that reduced gas exchange reduced grapevine vulnerability to water stress under projected conditions for economically important wine regions in North America and Europe (Dayer et al., 2022). Reducing gas exchange conserved soil water resources and extended the time required for vine water potentials to exceed critical thresholds for hydraulic damage (i.e., a 100 % loss of leaf hydraulic conductivity). However, it is unknown whether the traits defined as optimal in Dayer et al., 2022, which maximized the time to reach critical water stress, would compromise the carbon supply for ripening or capacity for evaporative cooling to protect the leaves from heat damage. Grapevine carbon demand is typically larger under high evaporative demand, since berry sugar accumulation occurs in the hottest period of the growing season (Vivin et al., 2002), and hotter US wine regions are typically managed for higher yields than premium regions (CDFA, 2020). Grapevines have also been shown to open stomata during heatwaves to facilitate evaporative cooling (Sadras et al., 2012; Soar et al., 2009). Thus, accounting for the trade-offs among carbon gain, avoiding water stress, and cooling is crucial to identify the most adaptive stomatal traits for future conditions.

Functional-structural plant models (FSPMs), which predict whole-plant performance from spatially explicit plant architecture and mechanistic organ-level physiology, provide a powerful approach to evaluate complex trait impacts on plant function (Soualiou et al., 2021; Vos et al., 2010). Here, we used an FSPM developed for grapevine to test how stomatal traits impact vine gas exchange, water potentials, and temperatures under different management practices (i.e., trellising systems and irrigation regimes) and climate change scenarios (Albasha et al., 2019). We focused on traits characterizing the relationship between stomatal conductance (g_s) and leaf water potential (Ψ_L): g_{max}, the maximum stomatal conductance in the absence of water stress (i.e., g_s at $\Psi_L = 0$ MPa), and g_s Ψ_{50}, the water potential threshold for 50 % stomatal closure (i.e., Ψ_L at $g_s = g_{max}/2$) (Guyot et al., 2012). A higher g_{max} increases the maximum rate of transpiration, photosynthesis, and evaporative cooling. A more negative g_s Ψ_{50} allows leaves to maintain greater gas exchange under water stress, while a higher g_s Ψ_{50} increases stomatal sensitivity to water stress and prevents strong declines in leaf water potentials and soil moisture.

We advanced previous work modeling the impacts of stomatal traits on grapevine performance by comparing impacts between climate change scenarios and using a modeling approach that can account for differences in management practices. Previous work focused on the extreme Representative Concentration Pathway (RCP) 8.5 scenario, where atmospheric CO_2 concentrations continue to increase over the next century (Dayer et al., 2022; van Vuuren et al., 2011). RCP 8.5 is increasingly considered to be implausibly extreme (Pielke Jr et al., 2022, but see Schwalm et al., 2020), so we compared trait impacts under RCP 8.5 and 4.5, an intermediate scenario where CO_2 concentrations stabilize by mid-century (van Vuuren et al., 2011). We also used the FSPM to account for differences in management that could impact trait relationships with vine water, carbon, and energy balance. We compared Napa Valley, which has an optimal climate for premium wine, to the southern San Joaquin Valley (SJV), which is one of the hottest and most productive US wine regions, accounting for a nearly third of US winegrape production. SJV growers typically use greater irrigation and larger canopies trained to weeping, rather than upright, trellising systems to support large yields and prevent overexposure (Gladstone and Dokoozlian, 2003; Williams et al., 2022). Previous work modeled trait impacts using a "big-leaf" canopy approximation (Dayer et al., 2022), which cannot account for the impacts of complex canopy architecture on vine carbon and water fluxes or temperatures (Bailey et al., 2016; Prieto et al., 2012), and assumed vines were unirrigated, which is rare in the US wine regions and could overestimate vulnerability to water stress. We parameterized the FSPM with the range of trait values reported across grape cultivars (Bartlett and Sinclair, 2021) and the values that optimized the avoidance of water stress in Dayer et al. (2022). We identified the traits that 1) minimized total vine transpiration and water stress while 2) maintaining historical levels for vine carbon gain, which we assumed was an adequate carbon supply for fruit production, and 3) avoiding temperature thresholds for heat damage to photosynthesis. We tested whether these values differed between climate change scenarios and premium and high-production regions, to provide insight into how grape breeding efforts should be tailored to different industry sectors and account for uncertainty in climate projections.

2. Methods

2.1. Model overview

We supplied six stomatal trait parameterizations and three climate scenarios for two California wine regions to HydroShoot to evaluate the impacts on vine gas exchange and heat and water stresses. HydroShoot is described in detail in Albasha et al. (2019). Briefly, the model uses three-dimensional (3-D) vine architecture, plant physiology traits, and soil and atmospheric conditions as inputs for three modules (*hydraulics, energy budget*, and *gas exchange*) that calculate water potential, temperature, and gas exchange rates for individual leaves at an hourly timestep. Vine architecture is defined by supplying 3-D coordinates, diameters, and topological connections for each plant segment (i.e., shoot internode, petiole, and leaf). The *hydraulics* module uses the Ohm's law analogy to calculate the water flux and water potential for each vine segment *i*, assuming that the hydraulic conductivity of each segment (K_i) varies with its water potential (Ψ_i) following a sigmoidal vulnerability curve. The *energy budget* module calculates temperature for each leaf *l* (T_l), assuming that leaves gain energy from absorbed shortwave solar radiation ($R_{g,l}$) and thermal longwave irradiance from the sky, soil, and nearby leaves, lose energy through thermal longwave emission and transpiration (latent heat flux), and exchange energy with the air through thermal conduction-convection (sensible heat flux). The *gas exchange* module calculates the stomatal conductance to CO_2 for each leaf *l* ($g_{s,CO2,l}$) following a modified model of (Leuning, 1995):

$$g_{s,CO_2,l} = g_{s0,CO_2} + m_0 \frac{A_{n,l} + R_{d,l}}{(c_{i,l} - \Gamma)\left(1 + \left(\frac{\Psi_l}{\Psi_{crit,leaf}}\right)^n\right)} \quad (1)$$

where $g_{s0,CO2}$ is the residual conductance to CO_2, m_0 and n are shape parameters, c_i is intercellular CO_2 concentration, A_n is net carbon assimilation, and R_d is mitochondrial respiration. Stomatal conductance is assumed to vary sigmoidally with leaf water potential (Ψ_l), and $\Psi_{crit,leaf}$ is the Ψ_l threshold for a 50 % decline in stomatal conductance. A_n is calculated from the Farquhar model, assuming that the biochemical parameters depend on leaf temperature and nitrogen content. Leaf nitrogen content is assumed to vary across the canopy with light exposure, which is quantified following Prieto et al. (2012) as the mean photosynthetic photon flux density over the previous 10 days for each leaf ($PPFD_{10,l}$). Each module uses outputs from the others as inputs, and thus an iterative procedure is used to solve all three.

Leaf-level gas exchange is then summed to calculate whole-vine net carbon assimilation (A_{plant}) and transpiration (E_{plant}). The *soil* module then updates the soil volumetric water content by subtracting E_{plant} and, where applicable, adding drip irrigation water, and uses supplied moisture-retention curve parameters to calculate soil water potential (Ψ_{soil}). The soil is represented as a single hydraulic element, and the soil volume occupied by each vine is equal to the vine × row spacing multiplied by soil depth (2 m) and the percent of soil volume occupied by roots (i.e., rhizosphere coefficient, 65 %) (see section "*Vine architecture, vineyard design, and irrigation*" and Table S1 for details).

2.2. Stomatal trait parameterization

We defined six stomatal trait parameterizations by varying the maximum stomatal conductance to water vapor (g_{max}) at 25 °C and the leaf water potential threshold for 50 % stomatal closure (g_s Ψ_{50}). Five parameterizations were defined from a meta-analysis of stomatal traits compiled for 21 cultivars from 8 studies where field-grown vines were monitored for midday stomatal conductance (g_s) and leaf water potential (Ψ_{MD}) over the growing season (Bartlett and Sinclair 2021). These cultivars capture a wide range of geographic and climate associations (e.g., mean growing season temperatures for each cultivar ranged from 15.8 to 20.2 °C, capturing 47 % of the range from 14.7 to 24.1 °C across the 120 most planted cultivars worldwide) (Anderson and Nelgen, 2020). The meta-analysis standardized the calculation of the stomatal traits by fitting exponential ($g_s = ae^{-b\Psi_{MD}}$), sigmoidal $\left(g_s = \frac{a}{1+e^{-\left(\frac{\Psi_{MD}-c}{b}\right)}}\right)$, logistic $\left(g_s = \frac{a}{1+\left(\frac{\Psi_{MD}}{c}\right)^b}\right)$, and linear ($g_s = a + b\Psi_{MD}$) relationships between g_s and Ψ_{MD} and using Aikake Information Criterion corrected for small sample sizes (AICc) to identify the best-fit model for each cultivar (Burnham and Anderson, 2010). The best-fit models were used to calculate g_{max} as the g_s value at $\Psi_{MD} = 0$ MPa and g_s Ψ_{50} as the Ψ_{MD} value where $g_s = g_{max}/2$ (Table 1). We then defined a baseline scenario, where g_{max} and g_s Ψ_{50} equal the median values from the meta-analysis, and four high or low g_{max} or g_s Ψ_{50} scenarios, where each trait is equal to its 95th or 5th percentile value (i.e., + g_{max}, - g_{max}, + g_s Ψ_{50}, and - g_s Ψ_{50}, respectively) (Table 2, Fig. 1).

The sixth parameterization used the highest-performing values from a grapevine stomatal optimization experiment (Dayer et al., 2022). This study used the SurEau physiology model to determine the number of days without irrigation required for leaf water potentials to reach thresholds for critical hydraulic damage (i.e., a 100 % loss of leaf hydraulic conductance) under historical and projected climatic conditions for six wine regions, including Napa and Paso Robles, a California wine region intermediate in temperature between Napa and Fresno. A detailed description of SurEau is provided in Cochard et al. (2021). Briefly, SurEau and Hydroshoot both use trait and environmental inputs to calculate leaf water potential, temperature, and gas exchange from hydraulic, energy budget, and gas exchange equations, but differ in the representation of vine architecture, with SurEau using a "big leaf" canopy approximation that does not account for heterogeneity in light exposure and leaf physiological function. Dayer et al., simulated >50,000 trait parameterizations and defined the 200 highest-performing ("elite") parameter combinations as those producing the longest times to reach the critical Ψ_l thresholds (2022). However, the "elite" stomatal parameters were calculated from g_s responses to pre-dawn water potential, rather than Ψ_{MD}. To calculate the "elite" parameters as a function of Ψ_{MD}, we fitted the relationship between the g_s and Ψ_l values that SurEau calculated at midday (12 PM) using the mean "elite" parameter values and historical climatic conditions for Napa as inputs (Gambetta, G. and Cochard, H., personal communication) (Fig. S1). We used this relationship to calculate g_{max} and g_s Ψ_{50} (Fig. 1).

For each simulation, g_s Ψ_{50} was supplied directly to HydroShoot as $\Psi_{crit,leaf}$. g_{max} was supplied by inverting Eq. (1) to calculate the m_0 value at which stomatal conductance to water vapor ($1.6g_{s,CO2}$) equaled g_{max}, assuming that $\Psi_l = 0$, leaf temperature = 25 °C, and $PPFD_{10}$ equaled the mean value across the canopy over the simulation period for each site.

Table 1
Stomatal trait values compiled from the literature for 20 winegrape cultivars (Bartlett and Sinclair, 2021) used to define the baseline, +/− g_{max}, and +/− g_s Ψ_{50} trait scenarios.

Cultivar	g_{max} (mmol $m^{-2}s^{-1}$)	g_s Ψ_{50} (MPa)	References
Aglianico	595	−1.42	Levin et al., 2020
Cabernet Sauvignon	382	−1.17	Speirs et al., 2013
Cabernet Sauvignon	474	−1.03	Speirs et al., 2013
Cabernet Sauvignon	489	−1.48	Levin et al., 2020
Carménére	353	−1.04	Villalobos-González et al., 2019
Carménére	375	−1.09	Villalobos-González et al., 2019
Cinsault	483	−1.47	Levin et al., 2020
Durif	483	−1.51	Levin et al., 2020
Friesa	480	−1.52	Levin et al., 2020
Grenache	337	−0.92	Schultz, 2003
Grenache	442	−0.96	Martorell et al., 2015
Grenache	477	−1.47	Levin et al., 2020
Malbec	468	−1.48	Levin et al., 2020
Montepulciano	86	−1.16	Tombesi et al., 2014
Montepulciano	291	−0.86	Tombesi et al., 2014
Montepulciano	466	−1.59	Levin et al., 2020
Petit Verdot	465	−1.50	Levin et al., 2020
Refosco	459	−1.40	Levin et al., 2020
Riesling	243	−1.25	Park, 2001
Sangiovese	99	−1.01	Tombesi et al., 2014
Sangiovese	182	−0.96	Tombesi et al., 2014
Sauvignon Blanc	733	−1.25	Naor et al., 1994
Souzão	444	−1.51	Levin et al., 2020
Syrah	282	−1.05	Schultz, 2003
Syrah	304	−1.05	Villalobos-González et al., 2019
Syrah	348	−1.23	Villalobos-Gonzalez et al., 2019
Syrah	438	−1.34	Levin et al., 2020
Tannat	426	−1.53	Levin et al., 2020
Tempranillo	439	−1.20	Martorell et al., 2015
Tempranillo	424	−1.54	Levin et al., 2020
Tinta Amarela	406	−1.55	Levin et al., 2020
Tinta Madeira	402	−1.38	Levin et al., 2020
Touriga Nacional	398	−1.27	Levin et al., 2020

Table 2
Parameter values for the six stomatal trait scenarios.

Scenario	g_{max} (mmol m^{-2} s^{-1})	g_s Ψ_{50} (MPa)
Baseline	425	−1.27
+ g_{max}	586	−1.27
- g_s Ψ_{50}	425	−1.56
- g_{max}	155	−1.27
+ g_s Ψ_{50}	425	−0.93
Elite	87	−0.85

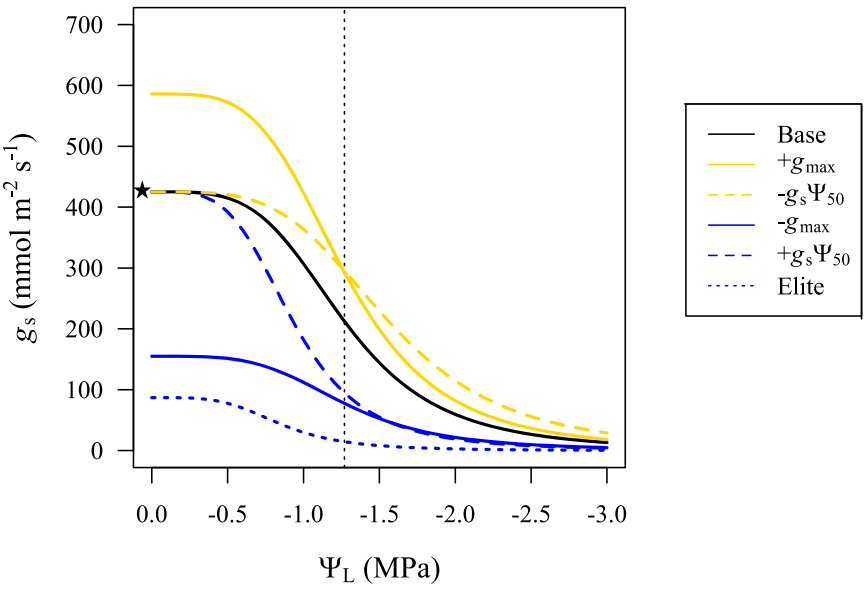

Fig. 1. Relationships between leaf water potential (Ψ_L) and stomatal conductance (g_s) produced by the six stomatal trait parameterizations (Table 1). Black line indicates average trait values reported across winegrape cultivars (baseline) (Bartlett and Sinclair, 2021). Black star indicates the baseline maximum stomatal conductance (g_{max} = 425 mmol m^{-2} s^{-1}) and dotted black line indicates the baseline Ψ_L threshold for a 50 % reduction in g_s from g_{max} (g_s Ψ_{50} = −1.27 MPa). Gold lines are water-spending trait parameterizations and blue lines are water-saving parameterizations. Dashed lines indicate parameterizations for the 95th and 5th percentile values reported across winegrape cultivars for g_s Ψ_{50} (+g_s Ψ_{50} = −0.93 MPa and -g_s Ψ_{50} = −1.56 MPa) and solid lines indicate parameterizations for 95th and 5th percentile values for g_{max} (+g_{max} = 586 mmol m^{-2} s^{-1} and -g_{max} = 155 mmol m^{-2} s^{-1}). Dotted blue line indicates the "elite" traits that minimized water stress in Dayer et al. (2022) (g_{max} = 87 mmol m^{-2} s^{-1} and g_s Ψ_{50} = −0.85 MPa). (For interpretation of the references to color in this figure legend, the reader is referred to the web version of this article.)

All other model parameters are provided in Table S2.

2.3. Climate scenarios

We simulated vine physiology for the month following veraison. We assumed veraison dates varied between sites and climate scenarios based on temperature. We chose this period to capture the growing season period with the hottest, driest conditions and minimal canopy growth, since HydroShoot works on static canopy structures.

Historical climate data was collected from two weather stations in the California Irrigation Management Information System network (CIMIS, https://cimis.water.ca.gov/). The Oakville station (38.43 N, 122.41 W) represents the premium Oakville, Napa Valley region, and the Fresno State station (36.82 N, 119.74 W) represents the hot, high-producing southern San Joaquin Valley. Hourly measurements were compiled for the HydroShoot input variables air temperature (T_{air}, °C), relative humidity (*RH*,%), windspeed (u, m s^{-1}), and solar global radiation (*Rg*, W m^{-2}) from the earliest 20-year period available for both stations (1990–2010). We excluded values flagged as unrealistic or outside the 99.8 % confidence interval for historical values by CIMIS (< 1 % of total data). Values were averaged across years to produce a representative trajectory of hourly climate conditions.

The future climatic conditions projected for each site were compiled from the Cal-Adapt database (https://cal-adapt.org/). We focused on the four global climate models (GCMs) identified as priority models for California (CanESM2, CNRM-CM5, HadGEM2-ES, MIROC5) because these models capture the widest range of projected temperature and precipitation changes across the 32 models evaluated in the Coupled Model Intercomparison Project (CMIP5). CanESM2, CNRM-CM5, and HadGEM2-ES represent average, cooler/wetter, and warmer/drier scenarios, respectively, and MIROC5 predictions were the most distinct from the other 32 models (Pierce et al., 2018). Projections were used for the moderate Representative Concentration Pathway (RCP) 4.5 emissions scenario, where global emissions stabilize by 2040 then decline, and the extreme RCP 8.5 scenario, where global emissions continue to increase over the next century. Projections were downscaled to a 1/16° spatial resolution with localized constructed analogs (LOCA) methods (Pierce et al., 2015, 2014). The projections generate daily estimates for minimum and maximum T_{air} and *RH* and mean *Rg* and u. We extracted these values for the 20-year period at the end of the century (2079–2099) and averaged projections from all years and models to generate a representative trajectory of daily climate conditions.

We then downscaled the climate projections from daily to hourly using models fitted to the historical climate data. First, for each site s, we predicted hourly (h) values for T_{air} from the minimum and maximum values for each day d ($T_{min,d}$ and $T_{max,d}$), using the model from Linvill 1990

$$T_{air,h,d,s} = \left(T_{max,d,s} - T_{min,d,s}\right)\sin\left(\pi\frac{h - S_{d,s}}{L_{d,s} + \beta_s}\right) + T_{min,d,s} \quad (2)$$

where S_d is the daily time at sunrise, L_d is the day length, and β is a fitted parameter. This model is only applicable to daylight hours, so we used Eq. (2) to estimate T_{air} from 6 AM to 9 PM, and made the simplifying assumption that hourly T_{air} was constant and equal to $T_{min,d}$ overnight. We used the *chillR* package in *R* (v. 4.1.0) to determine $S_{d,s}$ and $L_{d,s}$ from the date and site latitude, and the *likelihood* package to fit β_s for the historical T_{air} measurements over each simulation period. The best-fit β_s values were then used to predict hourly T_{air} from the RCP 4.5 and 8.5 projections for $T_{min,d}$ and $T_{max,d}$.

We used the same procedure to fit β_s for hourly incident global radiation (*Rg*) and wind speed (u). The projections for these variables were only for daily means, so we estimated daily maximum and minimum values by assuming that the minimum daily *Rg* = 0 and, thus, the maximum *Rg* = 2 × mean *Rg*, and that the daily minimum windspeed was equal to historical values and, thus the maximum u = 2 × (mean–minimum u). This assumption is consistent with observed trends for windspeed; in the western US, minimum daily u remained constant while maximum values increased from 1961 to 1990 (Klink, 1999). We then used Eq. (2) to predict hourly values from the daily maximum and minimum *Rg* and u. Finally, we used the air temperature estimated from

Eq. (2) to calculate hourly relative humidity

$$RH_{h,d,s} = RH_{\max,d,s} + \left(RH_{\min,d,s} - RH_{\max,d,s}\right)\left(\frac{T_{air,h,d,s} - T_{\min,d,s}}{T_{\max,d,s} - T_{\min,d,s}}\right) \quad (3)$$

from daily minimum and maximum values ($RH_{\min,d}$ and $RH_{\max,d}$) (Waichler and Wigmosta, 2003).

We assumed that atmospheric CO_2 concentrations are 400 ppm for historical conditions and 534 and 837 ppm for RCP 4.5 and 8.5, which were calculated as the mean projected CO_2 concentrations from 2070–99 for each RCP (van Vuuren et al., 2011).

2.4. Phenology

We assumed that phenology would advance with temperature under future climatic conditions. We used the Grapevine Flowering Veraison (GFV) model from Parker et al. (2011) to calculate veraison dates. We used the average historical climate data to calculate the growing degree days (GDD) from Jan 1 to typical dates reported for budbreak and veraison for Cabernet Sauvignon in Napa (Apr 1 and Jul 30) and French Colombard in the SJV (Mar 25 and Jul 15), which are the most planted varieties in each region (CDFA, 2020). Following the GFV model, GDD were calculated with a base temperature of 0 °C. We assumed the GDD thresholds were constant and estimated veraison dates for RCP 4.5 and 8.5 as the dates where GDD crossed these thresholds. Predicted veraison dates shifted from July 30 to July 16 and July 6 for RCP 4.5 and 8.5 in Napa and from July 15 to July 2 and June 25 in the SJV.

2.5. Vine architecture, vineyard design, and irrigation

Each site was parameterized with a vine architecture capturing representative local trellising systems (Fig. 2). The Napa simulations used the bilateral cordon vertically shoot-positioned (VSP) canopy mockup from Albasha et al. (2019), which was digitized with an electromagnetic 3D digitizer (Fastrak, Polhemus Inc., Colchester, VT, USA) from a mature (10-yo), field-grown Syrah vine at veraison in the Montpellier, France INRAE research vineyard (3°53′E, 43°37′N). The SJV simulations used a bilateral cordon California Sprawl architecture, which was manually mocked-up using HydroShoot's vine architecture library to reproduce the canopy properties reported by (Gladstone and Dokoozlian, 2003). California Sprawl trellising allows the shoots to hang downwards to shade and cool the fruit zone, while VSP trellising holds the shoots upright to increase light exposure in the fruit zone. Canopy area and vine × row spacing were typical for each region (4 m^2 at 1.8 × 2.1 m for Napa and 12 m^2 at 2.2 × 3.0 m for the SJV). We assumed that total root length per vine, which affects the root area available for water uptake and, thus, the hydraulic conductivity of the root system, increased with canopy area so that the ratio of canopy to root area was constant (1000 m at Napa and 3000 m at the SJV) (Table S1). We simulated solar radiation assuming a north-south row orientation, which has been the standard for California (Goldammer, 2018).

We also simulated typical irrigation regimes for each region. Irrigation was applied at a rate of 3.8 L h^{-1} every 7 days in Napa to replace 60 % of cumulative whole-plant transpiration since the last irrigation, and every 3 days at 80 % replacement in the SJV (Williams, 2014; Williams et al., 2010). We made the simplifying assumptions that there was no precipitation over the simulation period and that both sites had the same soil depth (2 m) and soil type (clay loam), which determines the soil moisture-retention curve parameters of van Genuchten (1980), following the soil texture classes of Carsel and Parrish (1988). We assumed all simulations began with a Ψ_{soil} of −0.6 MPa, which is a typical target for soil water depletion by veraison (Deloire et al., 2020; Van Leeuwen et al., 2009).

2.6. Model output analysis

We supplied the trait and climate parameterizations to HydroShoot and calculated gas exchange, water potential, and temperature at the leaf level at an hourly timescale over each 30-day simulation period. We summed E and A_n for all leaves to calculate whole-plant transpiration (E_{plant}) and net carbon gain (A_{plant}) at an hourly timescale and over the entire simulation period. We calculated whole-plant water-use efficiency (WUE) as A_{plant}/E_{plant} over the simulation period. We characterized the stomatal behavior driving the plant water and carbon fluxes by calculating the mean canopy g_s at the hottest time of day (3 PM) over the simulation period. We quantified the impacts of the trait and future climate scenarios on gas exchange by calculating the percent difference from total E_{plant}, A_{plant}, and WUE and mean g_s for baseline stomatal traits under historical conditions (e.g., for trait scenario i and climate scenario j, $\Delta E_{plant,i,j} = 100\ \frac{E_{plant,i,j} - E_{plant,\ baseline,\ historical}}{E_{plant,\ baseline,\ historical}}$).

We quantified vine water and heat stress by calculating mean canopy leaf water potentials and temperatures at the hottest time of day (3 PM) at a daily timescale (Ψ_{canopy} and T_{canopy}) and over the simulation period ($\overline{\Psi}_{canopy}$ and $\overline{T}_{canopy}$). We measured the effectiveness of evaporative cooling by calculating the mean difference between air and canopy temperature. We also measured the impacts of the trait and climate scenarios on spatial and temporal variation in water and heat stress. To characterize spatial variation in stress within the canopy, we calculated the mean percent of canopy area with leaf water potentials below the

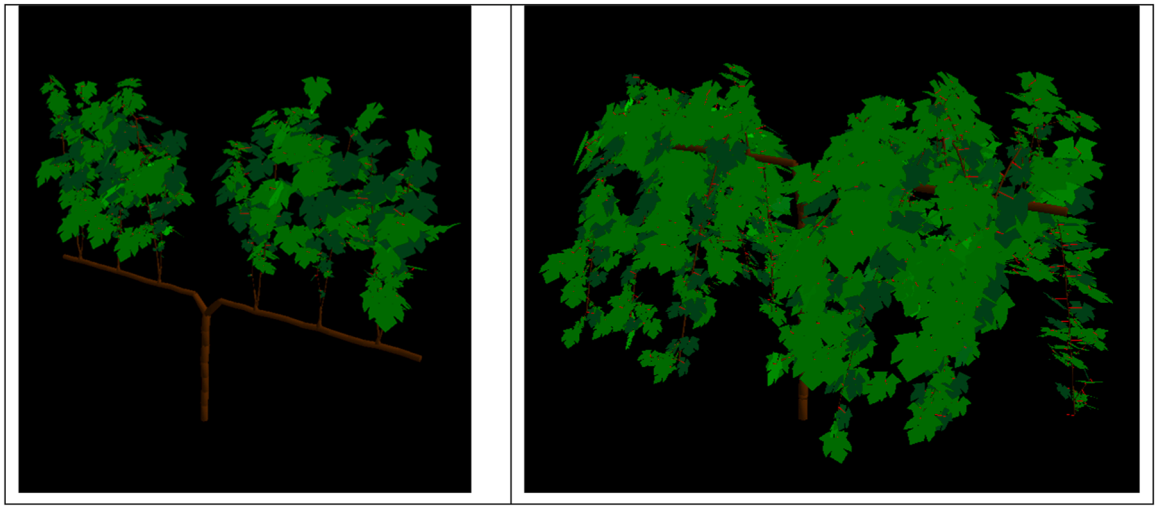

Fig. 2. VSP (left) and California Sprawl (right) canopy mock-ups used for the Napa and San Joaquin Valley simulations, respectively.

threshold for turgor loss and wilting ($\overline{PLA}_{TLP}$), and with leaf temperatures greater than T_{air} ($\overline{PLA}_{Tair}$). The leaf water potential threshold for turgor loss (i.e., $TLP = -1.7$ MPa) was defined as the mean value from veraison to mid-ripening reported for eight winegrape cultivars grown under unirrigated field conditions in an arid Mediterranean wine region (Alsina et al., 2007). Finally, we characterized temporal variation in water and heat stress by calculating the number of days over the simulation periods where mean canopy water potentials (Ψ_{canopy}) were more negative than *TLP* and mean canopy temperatures (T_{canopy}) were higher than T_{air}.

3. Results

3.1. Climate change is predicted to make California wine regions warmer and drier

The San Joaquin Valley (SJV) is warmer and less humid, with greater light exposure, than Napa, and climate change is projected to make both regions warmer and drier. Maximum daily temperatures over the simulated month after veraison increased from 29.1 ± 0.2 °C (mean ± standard error) to 33.5 ± 0.1 °C and 35.6 ± 0.1 °C for RCP 4.5 and 8.5 in Napa and from 34.7 ± 0.1 °C to 40.9 ± 0.1 °C and 42.3 ± 0.2 °C in the SJV (Fig. 3a,b). Minimum daily relative humidity decreased from 42.0 ± 0.6 % to 26.1 ± 0.2 % and 27.2 ± 0.2 % for RCP 4.5 and 8.5 in Napa and from 27.5 ± 0.2 % to 19.3 ± 0.1 % and 24.4 ± 0.2 % in the SJV (Fig. 3c,d). Maximum daily solar radiation decreased from 872 ± 5 to 836 ± 5 and 846 ± 6 W m^{-2} for RCP 4.5 and 8.5 in Napa, and from 900 ± 3 to 889 ± 3 and 884 ± 4 W m^{-2} in the SJV (Fig. 3e,f). Maximum daily windspeed was similar between sites, and projected to increase from 3.4 ± 0.1 to 4.3 ± 0.1 and 4.1 ± 0.1 m s^{-1} in Napa and from 3.2 ± 0.1 to 4.6 ± 0.1 and 4.3 ± 0.1 m s^{-1} in the SJV (Fig. 3g,h).

3.2. Extreme water-saving stomatal traits conserved water without compromising future carbon gain in Napa, but only under high CO_2 fertilization in the SJV

The impacts of the stomatal traits and climate change scenarios on vine gas exchange varied between wine regions (Fig. 4). In Napa, future conditions increased both total whole-plant transpiration (E_{plant}) and net carbon gain (A_{plant}) (Figs. 5, S2). The effects of warming dominated for RCP 4.5, increasing transpiration more than carbon gain and reducing water-use efficiency (WUE_{plant}) (e.g., for the baseline stomatal trait scenarios, RCP 4.5 increased E_{plant} by 50 % and A_{plant} by 36 % and decreased WUE_{plant} by 9 % compared to historical conditions) (Figs. 3, 5, S2). In contrast, the effects of CO_2 fertilization dominated for RCP 8.5. RCP 8.5 reduced mean daily stomatal conductance more strongly than RCP 4.5, which also made E_{plant} lower than for RCP 4.5 despite the higher temperatures (e.g., for the baseline traits, RCP 8.5 increased E_{plant} by 46 %, A_{plant} by 78 %, and WUE_{plant} by 22 % compared to historical conditions) (Figs. 5, 6, S2). These trends were similar, but the magnitude of climate change impacts on gas exchange were smaller in the SJV. For the baseline stomatal traits, RCP 4.5 only increased E_{plant} by 19 % and A_{plant} by 10 %, and decreased WUE_{plant} by 8 %, while RCP 8.5 decreased E_{plant} by 8 % and increased A_{plant} by 53 % and WUE_{plant} by 41 %, compared to historical conditions (Figs. 5, S3).

The stomatal traits had a stronger impact on transpiration than carbon gain, and thus shifting from baseline to water-saving traits improved water-use efficiency. The most extreme water-saving ("elite") traits conserved water but compromised carbon gain under historical conditions, while the effects on carbon gain under future conditions varied between sites. Under historical conditions, shifting from baseline to water-saving traits (i.e., a lower g_{max}, a less negative g_s Ψ_{50}, or both ("elite")) reduced E_{plant} by 19–64 % and A_{plant} by 5–33 % in Napa and E_{plant} by 20–55 % and A_{plant} by 10–38 % in the SJV (Figs. 5, S2–3), suggesting that selecting for these traits could reduce ripening capacity if historical conditions persist. Conversely, in Napa, under future climate conditions, CO_2 fertilization allowed the most extreme water-saving traits to reduce transpiration without notably compromising carbon gain. Shifting from baseline traits historically to "elite" traits in the future reduced E_{plant} by 38 % and A_{plant} by 3 % for RCP 4.5 and reduced E_{plant} by 37 % and increased A_{plant} by 35 % for RCP 8.5 (Fig. 5). In the SJV, the extreme water-saving "elite" traits also conserved water without reducing carbon gain for RCP 8.5, but not RCP 4.5. Shifting from baseline to "elite" traits reduced E_{plant} by 41 % and A_{plant} by 23 % for RCP 4.5, but reduced E_{plant} by 47 % and increased A_{plant} by 15 % for RCP 8.5, due to greater CO_2 fertilization (Fig. 5). Shifting from baseline to the most water-saving traits reported from existing cultivars (i.e., a lower g_{max} or higher g_s Ψ_{50}) instead allowed for moderate water conservation with only minor declines in carbon gain for RCP 4.5. The lower g_{max} scenario reduced E_{plant} by 10 % and A_{plant} by 0.5 %, and the higher g_s Ψ_{50} scenario reduced E_{plant} by 4 % and increased A_{plant} by 2 % (Fig. 5). At both sites, shifting to more water-spending traits was detrimental, by increasing transpiration more than carbon gain, and was not necessary to maintain historical carbon gain, since CO_2 fertilization increased future carbon gain for the baseline traits. Overall, these findings suggest that selecting for extreme water-saving traits would be an effective strategy to reduce water use in Napa, and in the SJV under the most extreme emissions scenario, while intermediate water-saving traits would be needed to avoid compromising ripening in the SJV under moderate emissions.

3.3. All water-saving traits protected vines from severe water stress under future conditions

Vines in the SJV experienced more water stress than in Napa, and climate change exacerbated water stress at both sites (Figs. 7, S4–5). RCP 4.5 induced the strongest water stress, since minimum daily relative humidity was projected to be lowest for this scenario in the month after veraison (Fig. 2c,d), and the higher CO_2 concentrations for RCP 8.5 allowed for more conservative stomatal behavior (Fig. 6). For baseline stomatal traits, mean canopy leaf water potentials at the hottest time of day over the simulation periods ($\overline{\Psi}_{canopy}$) decreased from −1.16 to −1.46 and −1.41 MPa for RCP 4.5 and 8.5 in Napa, and from −1.66 to −1.80 and −1.67 MPa in the SJV (Figs. 7, S4–5). The number of days where mean canopy water potential at the hottest time of day declined below thresholds for leaf turgor loss and wilting (i.e., $TLP = -1.7$ MPa) increased from 0 to 4 and 2 for RCP 4.5 and 8.5 in Napa, and from 8 to 29 and 8 days in the SJV (Fig. 7). On average, the percent of the canopy area with leaf water potentials below *TLP* at the hottest time of day increased from 0 % to 15 % and 8 % for RCP 4.5 and 8.5 in Napa, and from 46 % to 67 % and 42 % in the SJV (Fig. 7). Thus, future conditions increased the duration of severe water stress and the spatial extent in the canopy, especially in the SJV, exacerbating the risk of fruit dehydration and sunburn.

Shifting from baseline to water-saving traits protected the canopy from severe water stress under future conditions. All three water-saving trait scenarios made $\overline{\Psi}_{canopy}$ less negative under future conditions than for baseline traits historically and avoided turgor loss and wilting, with the extreme "elite" traits producing the least negative water potentials. For all three trait scenarios, $\overline{\Psi}_{canopy}$ ranged from −1.22 to −0.87 MPa and −1.19 to −0.87 MPa for RCP 4.5 and 8.5 in Napa and from −1.52 to −1.14 MPa and −1.40 to −1.07 MPa in the SJV (Fig. 7, S4–5). Ψ_{canopy} remained above *TLP* every day and, on average, none of the canopy area experienced water potentials below *TLP*, for both sites and RCPs (Fig. 7). Conversely, shifting to water-spending trait scenarios strongly exacerbated water stress, reducing $\overline{\Psi}_{canopy}$ and increasing the duration and spatial extent of water potentials below *TLP* (Fig. 7). Altogether, these findings suggest that selecting for any of the water-saving trait values would be an effective strategy to protect vines from severe water stress under future conditions.

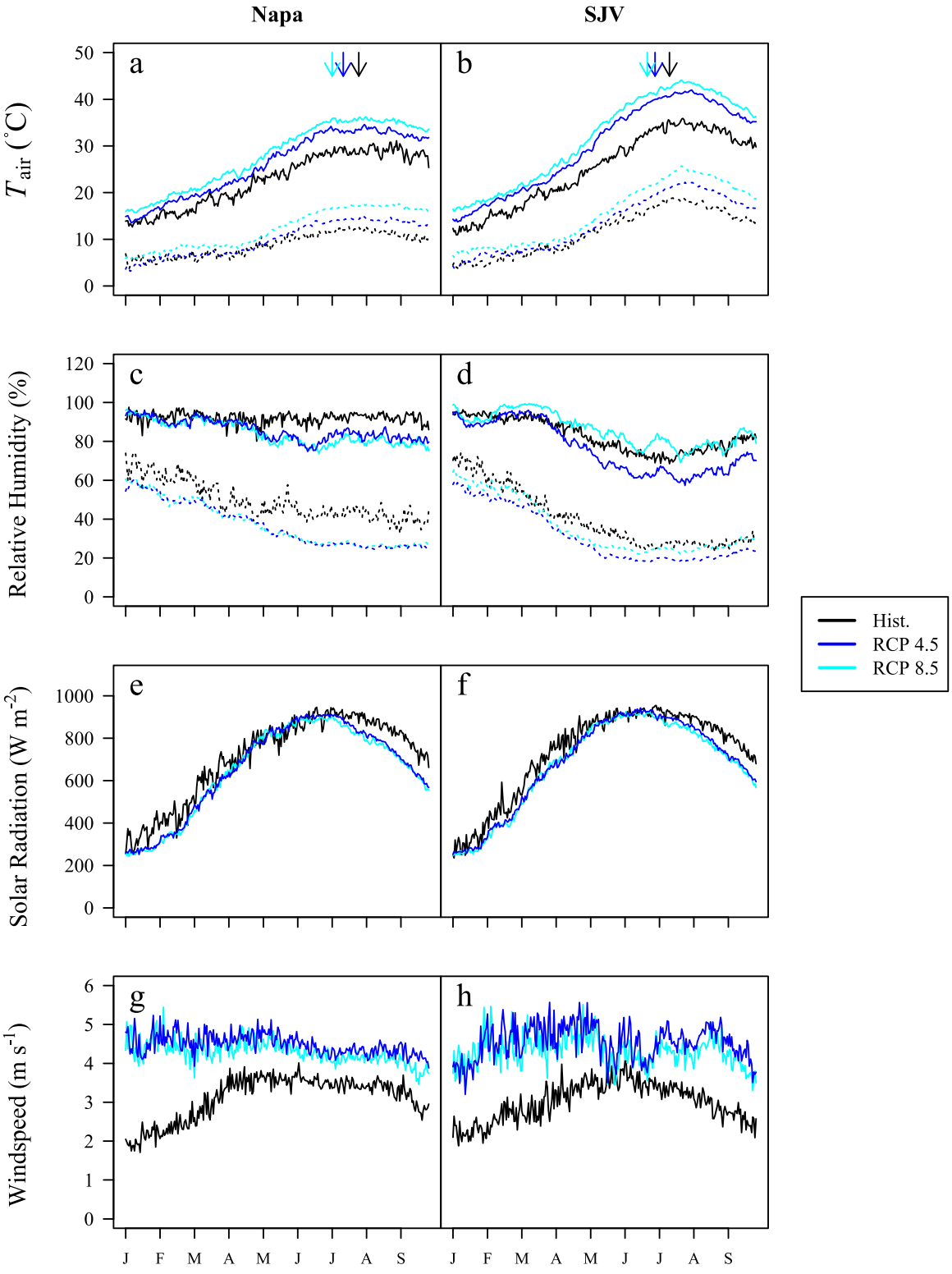

Fig. 3. Daily environmental conditions for each site and climate scenario. Left panels show conditions for Napa (a, c, e, g) and right panels for the southern San Joaquin Valley (b, d, f, h). Panels show maximum and minimum daily air temperature (T_{air}) (a, b) and relative humidity (c, d), maximum daily solar radiation (e, f), and maximum daily windspeed (g, h). Solid lines in panels a–d indicate maximum values and dotted lines indicate minimum values. Colors indicate climate scenarios (historical = black, Representative Concentration Pathway (RCP) 4.5 = blue, and RCP 8.5 = cyan). Each line is an average of a 20-year period (i.e., from 1990–2009 for historical conditions and 2079–99 for RCP 4.5 and 8.5). Historical conditions were measured by California Irrigation Management Information System (CIMIS) climate stations at Oakville in Napa (lat., lon. = 38.43, −122.41) and Fresno in the SJV (36.82, −119.74). RCP 4.5 and 8.5 conditions are global climate model projections for these sites, averaged from the four priority climate models for California, and accessed from the Cal-Adapt database. Phenology was assumed to adjust with climate, and the arrows indicate the start of the simulation period for each climate scenario. (For interpretation of the references to color in this figure legend, the reader is referred to the web version of this article.)

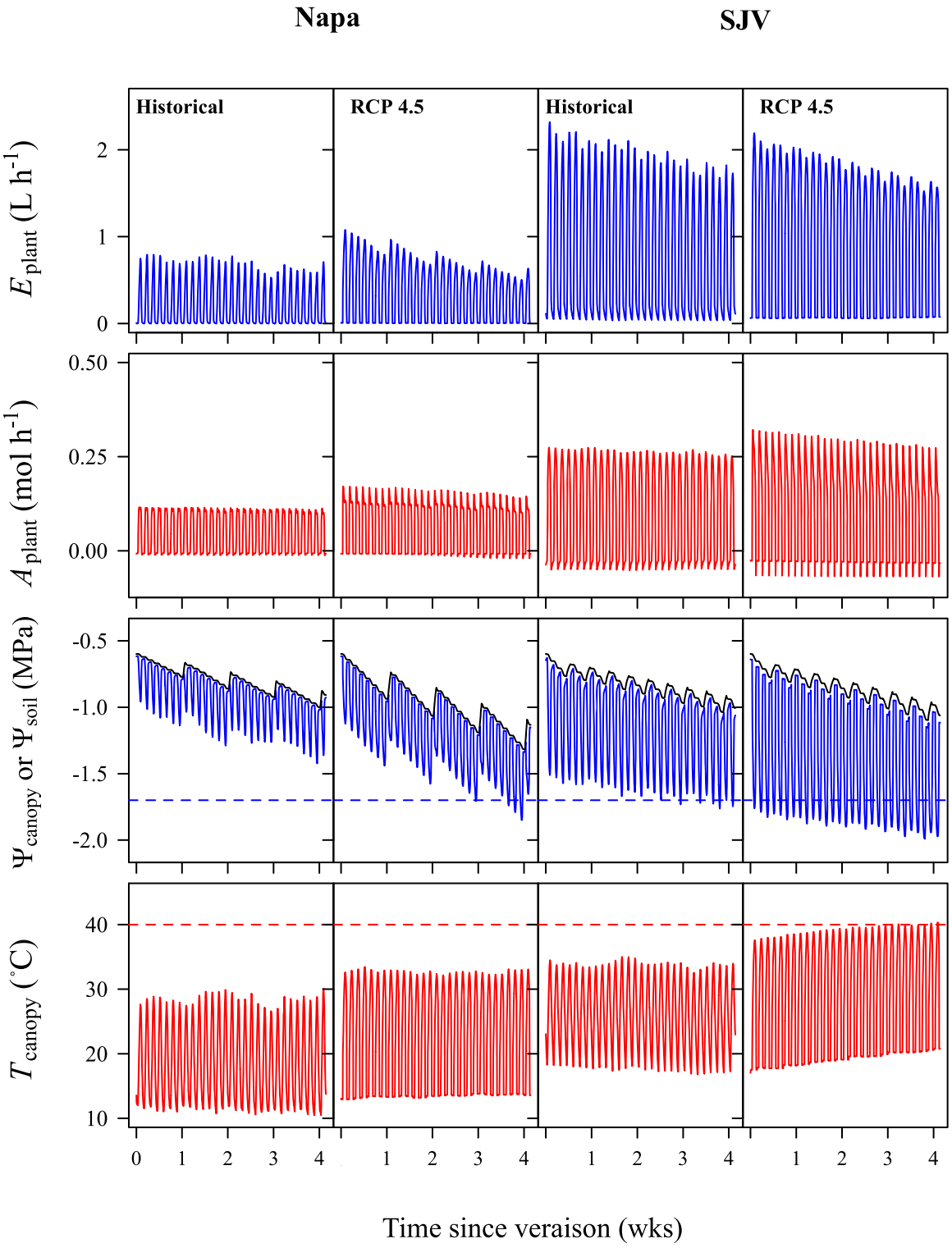

Fig. 4. Example demonstrating the impacts of site and climate scenario on model predictions for vine gas exchange, water potential, and temperature for the month after veraison. Simulations are for baseline stomatal trait values (g_{max} = 425 mmol m^{-2} s^{-1} and g_s Ψ_{50} = −1.27 MPa) in premium (Napa) and hot (SJV) California wine-growing regions under historical and moderate climate change (RCP 4.5) scenarios. Model predictions are whole-plant transpiration (E_{plant}) and net carbon assimilation (A_{plant}) rates, mean leaf and soil water potentials (Ψ_{canopy} and Ψ_{soil}), and mean canopy temperatures (T_{canopy}), at an hourly timescale over each simulation period (7/30–8/29 and 7/16–8/15 for historical and RCP 4.5 scenarios in Napa and 7/15–8/14 and 7/2–8/1 in the SJV). Black lines indicate soil water potentials, dashed blue lines indicate leaf water potential thresholds for wilting (i.e., −1.7 MPa), and dashed red lines indicate leaf temperature thresholds for photochemical damage (i.e., 40 °C). Warming and CO_2 fertilization increased vine transpiration and carbon gain rates, exacerbated soil drying and vine water stress, and increased canopy temperatures from historical to RCP 4.5 conditions. Higher evaporative demand and larger canopy size (i.e., 12 m^2 vs. 4 m^2) made gas exchange rates, water stress, and canopy temperatures larger in the SJV than Napa. Model predictions for all trait and climate scenarios are provided in Figs. S2–S5. (For interpretation of the references to color in this figure legend, the reader is referred to the web version of this article.)

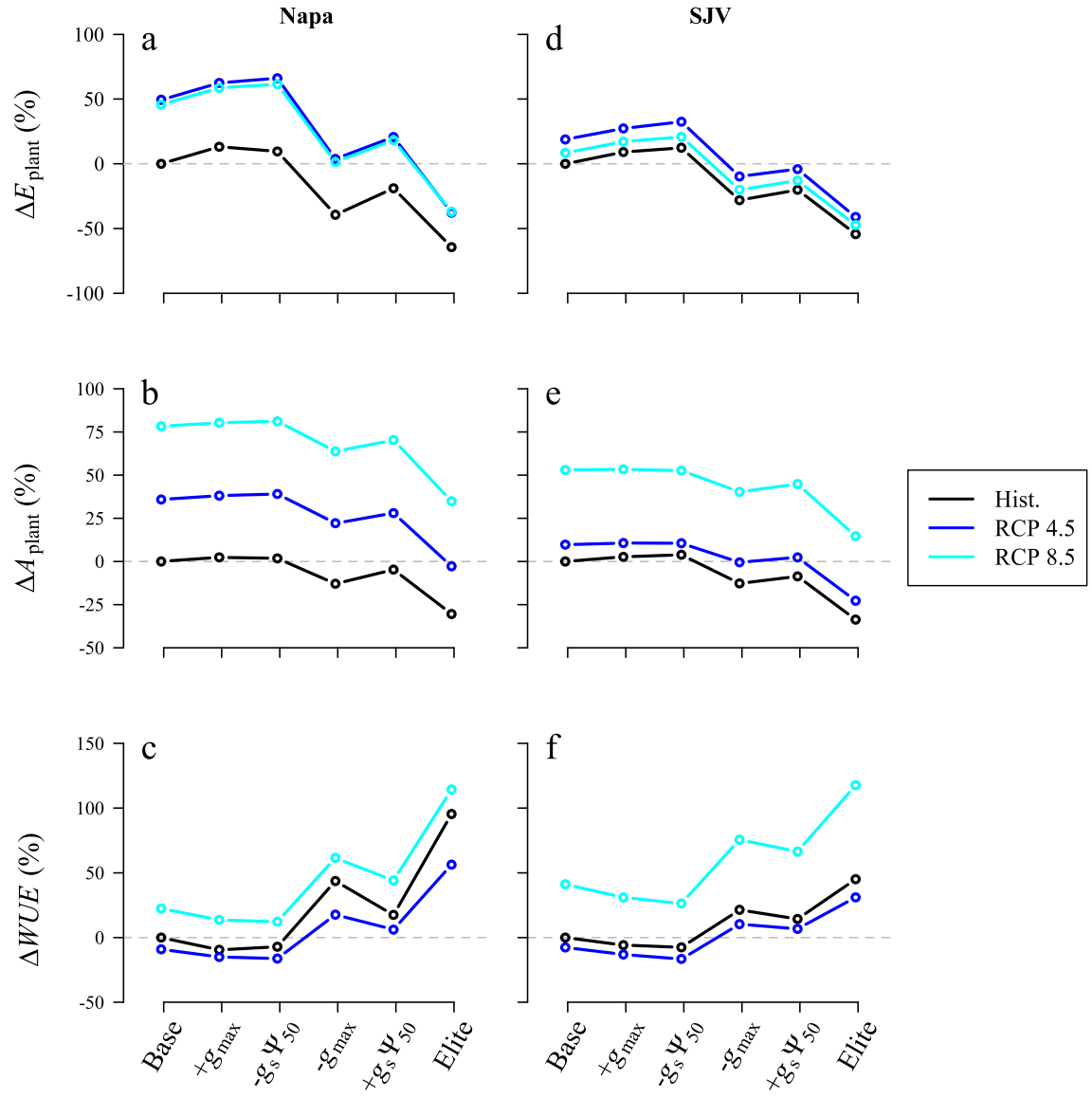

Fig. 5. Trait and climate impacts on total whole-plant transpiration (E_{plant}) (a, d), net carbon assimilation (A_{plant}) (b, e), and water-use efficiency (WUE) (c, f) over the simulated month after veraison. Impacts are measured as the percent difference from baseline traits under historical conditions (e.g., for trait scenario *i* and climate scenario *k*, $\Delta E_{plant,i,k} = 100\frac{E_{plant,i,k} - E_{plant,\ baseline,\ historical}}{E_{plant,\ baseline,\ historical}}$). Left panels show impacts for Napa (a, b, c) and right panels for the southern San Joaquin Valley (SJV) (d, e, f). Dashed lines indicate a percent difference of 0. Future conditions increased net carbon assimilation through CO_2 fertilization (i.e., atmospheric CO_2 concentrations = 400 ppm for historical scenarios, 534 ppm for RCP 4.5, and 837 ppm for RCP 8.5) (a, d), allowing for reductions in stomatal conductance that partly mitigated the effects of warming on transpiration (b, e). In the premium region (Napa), CO_2 fertilization allowed shifting from baseline to extreme water-saving ("elite") traits to maintain carbon gain above historical levels, while reducing transpiration, for both RCP 4.5 and 8.5. This was also the case for RCP 8.5 in the hot, high-production region (the SJV). However, these traits reduced net carbon gain below historical baseline levels at this site under the weaker CO_2 fertilization from RCP 4.5. Instead, shifting to moderate water-saving trait scenarios (i.e., -g_{max} and +g_s Ψ_{50}) allowed for reductions in transpiration without compromising carbon gain under these conditions.

3.4. Water-saving traits only slightly increased the risk of heat damage

Future conditions increased the simulated canopy temperatures. Mean temperatures remained below typical thresholds for photochemical damage (40 °C) in Napa but crossed these thresholds under future conditions in the SJV. For the baseline stomatal traits, mean canopy temperature at the hottest time of day, averaged over the simulation periods ($\overline{T}_{canopy}$), increased from 28.4 °C historically to 32.8 °C and 34.9 °C for RCP 4.5 and 8.5 in Napa and from 33.8 °C to 40.1 °C and 41.4 °C in the SJV (Figs. 8, S4–5). Vines were able to maintain evaporative cooling and reduce mean canopy temperatures below air temperature at the hottest time of day, though the water-saving traits slightly reduced cooling capacity and increased the risk of heat damage. Shifting from baseline traits under historical conditions to the "elite" traits under future conditions reduced mean canopy temperature depression (T_{canopy}–T_{air}) from −0.61 °C to −0.23 °C and −0.22 °C for RCP 4.5 and 8.5 in Napa and from −0.62 °C to −0.26 °C and −0.21 °C in the SJV (Fig. 8). The proportion of the canopy with leaf temperatures > 40 °C remained 0 % for all climate scenarios in Napa and increased from 0 % to 70 % and 99 % for RCP 4.5 and 8.5 in the SJV (Fig. 8). In contrast, shifting to water-spending traits slightly facilitated evaporative cooling, reducing mean T_{canopy}–T_{air} from −0.61 °C to −0.76 °C and −0.70 °C for RCP 4.5 and 8.5 in Napa and from −0.62 °C to −0.75 °C and −0.73 °C in the SJV (Fig. 8). The proportion of the canopy leaves with temperatures

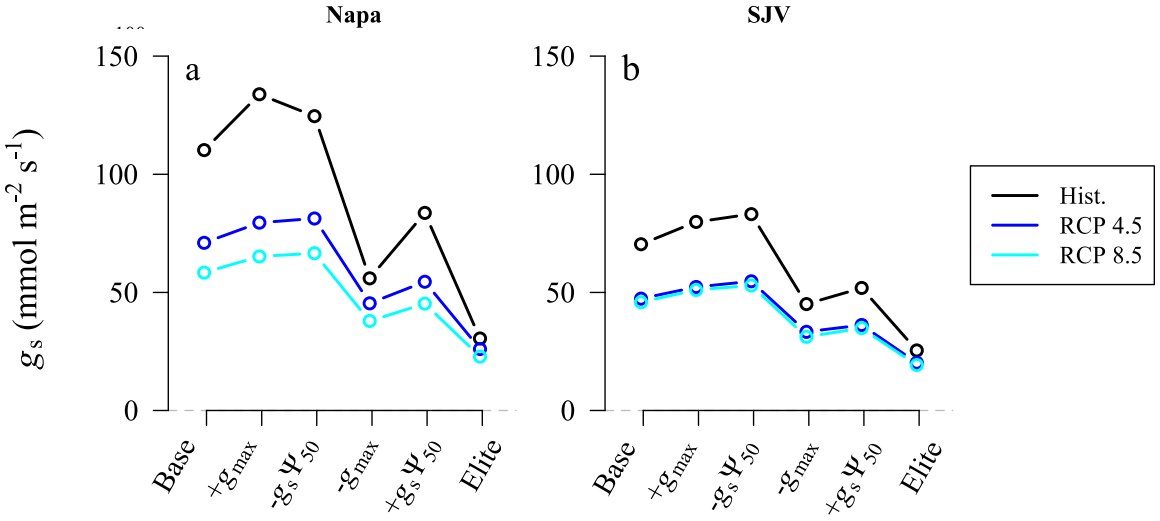

Fig. 6. Trait and climate impacts on mean daily stomatal conductance (g_s). CO_2 fertilization allowed for more conservative behavior under future conditions.

> 40 °C remained 0 % in Napa and increased to 50 % and 89 % for RCP 4.5 and 8.5 in the SJV for the -g_s Ψ_{50} scenario (Fig. 8). Overall, the stomatal traits had relatively small impacts on evaporative cooling capacity, suggesting that the water-saving traits would not substantively increase the risk of foliar heat damage under average future conditions, compared to water-spending traits.

4. Discussion

Shifting from average to water-saving stomatal traits reduced grapevine water use and water stress, but the traits that conserved water without compromising vine carbon gain varied between climate scenarios and wine regions. This study compared trait values from across the range reported for winegrape cultivars and values identified in previous work as minimizing vine water stress (i.e., maximizing the time required for vine water potentials to reach thresholds for a 100 % loss of leaf hydraulic conductance) (Dayer et al., 2022). The traits that minimized water stress–the "elite" water-saving traits (i.e., g_{max} = 87 mmol m^{-2} s^{-1} and g_s Ψ_{50} = −0.85 MPa)–compromised vine carbon gain (A_{plant}) under historical conditions but were beneficial under more future climate scenarios in the premium Napa region than the hot, high-production San Joaquin Valley (SJV). In Napa, shifting from baseline to "elite" traits reduced cumulative vine transpiration in the month after veraison (E_{plant}) below historical levels while maintaining historical carbon gain under both moderate (RCP 4.5) and severe (RCP 8.5) climate change scenarios (Fig. 5). In the SJV, shifting to "elite" traits maintained historical A_{plant} under RCP 8.5, but not RCP 4.5, reflecting a smaller CO_2 fertilization effect on photosynthesis under RCP 4.5 (Fig. 5). Instead, RCP 4.5 in the SJV favored the most water-saving traits reported across cultivars (i.e., g_{max} = 155 mmol m^{-2} s^{-1} or g_s Ψ_{50} = −0.93 MPa) (Fig. 5). Shifting to any of the three water-saving trait scenarios reduced vine water stress below historical levels (Fig. 7). The simulated canopy temperatures crossed thresholds for photochemical damage (40 °C) in the SJV, but the stomatal traits only slightly impacted cooling capacity (Fig. 8), indicating that stomatal trait selection alone is not sufficient to prevent heat stress and, thus, other strategies are needed. Overall, shifting to water-saving stomatal traits can mitigate climate change impacts by reducing irrigation demand and alleviating vine water stress without compromising carbon gain. Selecting for a range of trait values would provide plant material tailored to different growing regions and buffer uncertainty around future climate conditions.

Several factors made the "elite" traits beneficial under both future climate scenarios in Napa, but only under the most severe scenario in the SJV (RCP 8.5). First, the higher CO_2 concentrations increased photosynthesis, which allowed vines to reduce stomatal conductance, more strongly for RCP 8.5 than 4.5 (Figs. 5 and 6). This stronger reduction in mean g_s made E_{plant} lower, and, in turn, mean canopy water potentials ($\overline{\Psi}_{canopy}$) less negative, under RCP 8.5 than 4.5 (Figs. 5 and 7). Second, differences in evaporative demand and canopy structure made E_{plant} and A_{plant} more responsive to climate change in Napa, which made the "elite" water-saving traits more beneficial. Changes in relative humidity and evaporative demand were larger in Napa (Fig. 3). Mean *VPD* increased by 90 % and 120 % for RCP 4.5 and 8.5 in Napa and by 49 % and 41 % in the SJV compared to historical conditions, driving a larger increase in E_{plant} in Napa. Relationships between gas exchange, Ψ_L, and solar radiation (*Rg*) within the canopy suggest that the VSP canopy architecture also contributed to the greater increase in A_{plant} in Napa. The shorter shoots reduced vine hydraulic resistance and smaller canopy size reduced vine transpiration, producing a smaller range of leaf water potentials in the canopy (Figs. 2, S6). Thus, g_s and A were consistently high in sunlit leaves in the VSP canopy but limited by water stress in a significant fraction of sunlit leaves in the Sprawl canopy, which, in turn, limited photosynthetic responses to CO_2 fertilization (Fig. S7). Thus, CO_2 fertilization increased WUE without compromising carbon gain in both regions for RCP 8.5 and in Napa for RCP 4.5, but could not prevent substantive reductions in carbon gain in the SJV for RCP 4.5.

The most planted cultivars in California have more water-spending traits than average, making selecting for water-saving traits a valuable strategy for this area. Cabernet Sauvignon and Chardonnay account for 40 % of winegrape bearing area and exhibit trait values similar to the –g_s Ψ_{50} scenario (i.e., g_{max} = 489 and 445 mmol m^{-2} s^{-1} and g_s Ψ_{50} = −1.48 and −1.57 MPa, respectively) (CDFA, 2022; Levin et al., 2020) (Fig. S8). Compared to –g_s Ψ_{50} under historical conditions, the most water-saving traits that produced minimal (< 5 %) reductions in A_{plant} were the "elite" traits for both climate scenarios in Napa and +g_s Ψ_{50} for RCP 4.5 and the "elite" traits for RCP 8.5 traits in the SJV. Shifting from –g_s Ψ_{50} to these traits reduced E_{plant} by 43 % for both climate scenarios in Napa and by 15 % for RCP 4.5 and 53 % for RCP 8.5 in the SJV (Fig. S9). Vine transpiration is a significant component (~50 %) of total vineyard evapotranspiration, making selecting for water-saving traits a promising strategy to reduce irrigation demand, which is crucial to adapt agriculture to the reduced irrigation availability projected under climate change (Burchard-Levine et al., 2022; Darouich et al., 2022; Wilson et al., 2016). Previous work identified the "elite" traits as optimal for minimizing water stress, but only focused on RCP 8.5, which is increasingly considered to be implausibly extreme (Burgess et al., 2021;

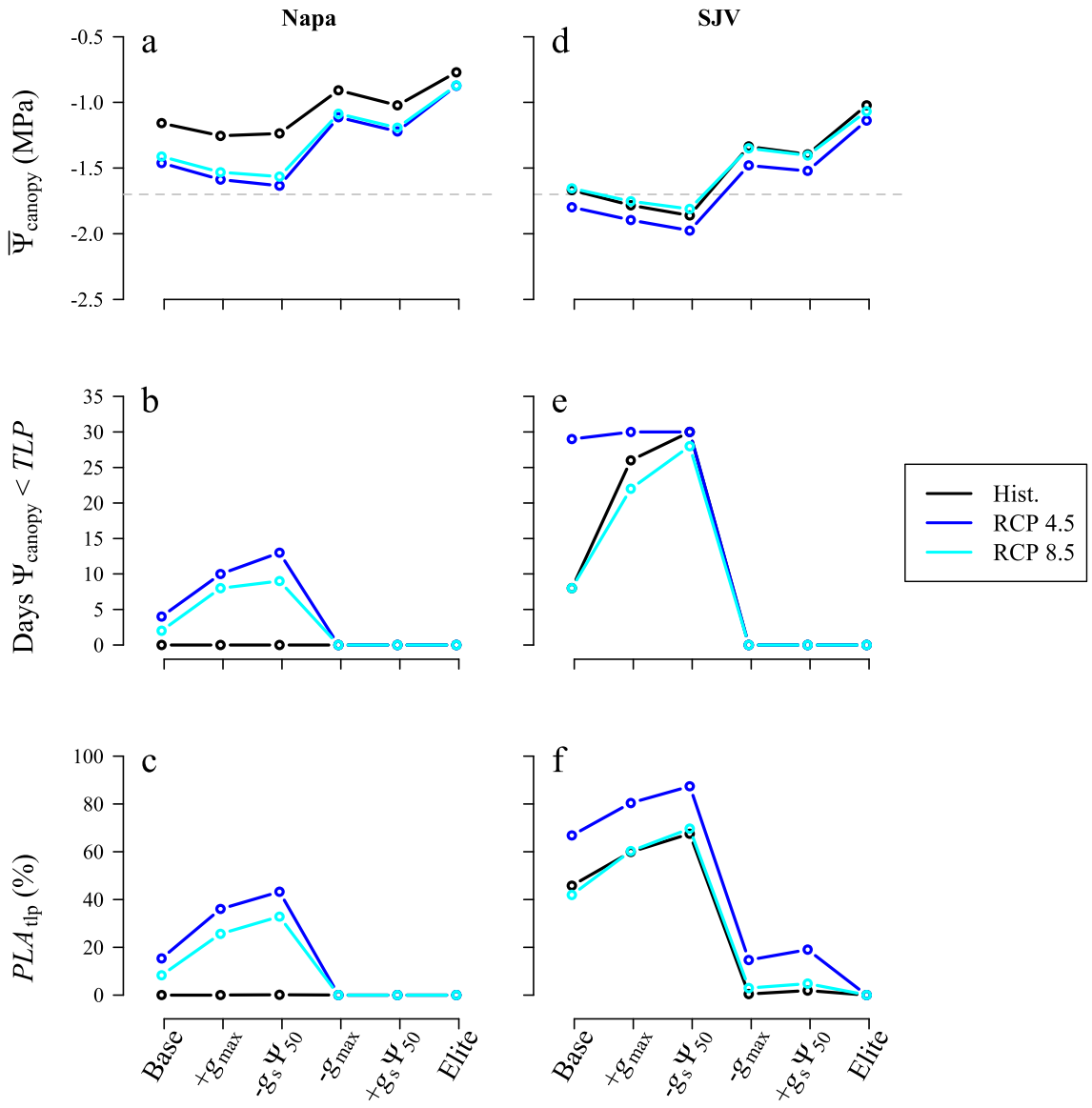

Fig. 7. Stomatal trait and climate impacts on vine water stress. Top panels (a and d) show the mean canopy water potential at the hottest time of the day (3PM) over each simulation period ($\overline{\Psi}_{canopy}$). Middle panels (b and e) show the number of days with daily mean canopy water potentials below leaf water potential thresholds for turgor loss and wilting (i.e., $TLP = -1.7$ MPa, dashed lines). Bottom panels (c and f) show the mean percent of canopy area with leaf water potentials below *TLP* ($\overline{PLA}_{tlp}$). Colors indicate climate scenarios. Left panels show values for Napa (a–c) and right panels show the SJV (d–f). Future conditions, especially RCP 4.5, reduced mean water potentials (a, d), increased the number of days with canopy water potentials below *TLP* (b, e), and increased the proportion of canopy area with leaf water potentials below *TLP* (c, f). Shifting from baseline to water-saving stomatal traits strongly reduced vine water stress. For these traits, $\overline{\Psi}_{canopy}$ under future conditions was less negative (a, d) and the duration of severe water stress (b, e) and the proportion of the canopy experiencing severe water stress (c, f), than for baseline traits under historical conditions. (For interpretation of the references to color in this figure legend, the reader is referred to the web version of this article.)

Pielke Jr et al., 2022). Developing grapevines with a range of trait values between "elite" to -g_{max} or +g_s Ψ_{50} scenarios would reduce risk from uncertainty by creating a "portfolio" of plant material tailored to different climate scenarios and growing regions.

While the genetic basis of stomatal behavior is complex and not well understood, and plasticity can significantly influence stomatal traits, gas exchange has a relatively high heritability in grape, suggesting that it is plausible to select for water-saving grapevines (Coupel-Ledru et al., 2014; Lavoie-Lamoureux et al., 2017; Sorek et al., 2020). There is relatively little market demand for new grape cultivars, but conventional breeding could be used to improve stomatal behavior in existing cultivars, if there is enough clonal diversity in the stomatal traits. Significant clonal differences in g_s have been observed in a few cultivars (i.e., Tempranillo and Monastrell), but, to the best of our knowledge, clonal diversity in gas exchange has never been measured for the main cultivars in California (Romero et al., 2023; Tortosa et al., 2020). Genetic engineering has been proposed as a faster alternative to breeding, and as a strategy to precisely target specific traits. While many genes are expected to determine g_s Ψ_{50} and g_{max}, transformations targeting single genes have successfully reduced g_s in grapevine and other species (Caine et al., 2019; Clemens et al., 2022). Future work should use clones or transformed plant material to experimentally test model predictions for how variation in stomatal traits in otherwise genetically similar plants impacts whole-plant gas exchange, growth, and ripening.

Conversely, several limitations to our modeling approach could overestimate the benefits of the water-saving traits. First, fluxes were

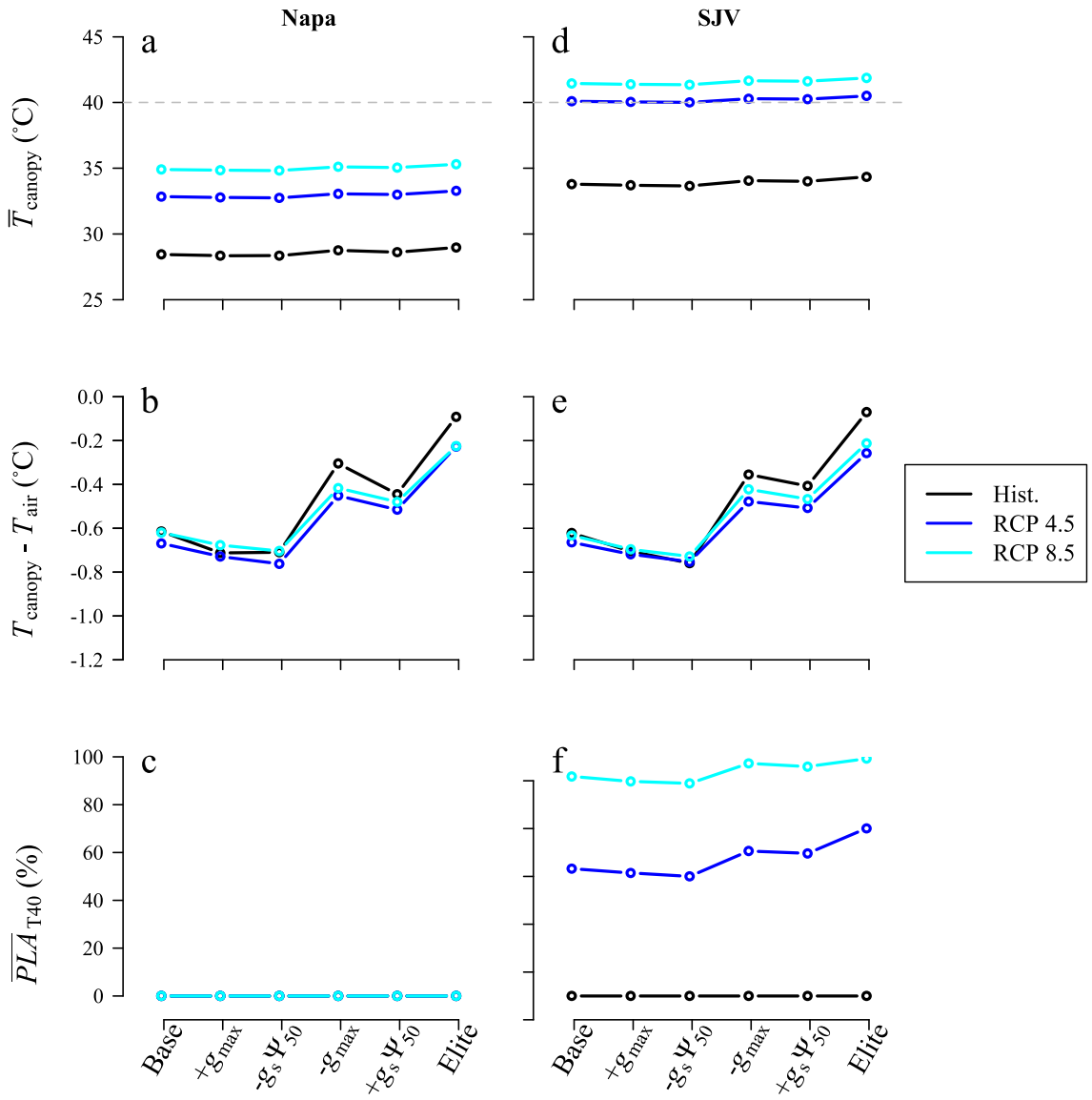

Fig. 8. Trait and climate impacts on heat stress. Top panels (a and d) show the mean canopy temperature over the month after veraison at the hottest time of day (3PM) ($\overline{T}_{canopy}$) for each stomatal trait parameterization. Dashed lines indicate approximate thresholds for persistent photochemical damage (40 °C). Middle panels (b and e) show mean differences between canopy and air temperature (T_{air}). Bottom panels (c and f) show the mean percent of canopy area with leaf temperatures > 40 °C ($\overline{PLA}_{T40}$). Left panels are from Napa (a–c) and right panels are from the SJV (d–f). Warming increased mean canopy temperatures under future conditions (a, d). Canopy temperatures remained well below 40 °C under future conditions in Napa (a), but crossed this threshold in the SJV (d). Evaporative cooling maintained cooler canopy than air temperatures for all trait and climate scenarios (b, e), though shifting from baseline to water-saving traits slightly reduced cooling capacity. For the hottest scenario, RCP 8.5, shifting from baseline to "elite' traits reduced mean T_{canopy}–T_{air} from −0.62 to −0.23 °C in Napa and from −0.63 °C to −0.21 °C in the SJV (b, e), while the proportion of the canopy with leaf temperatures > 40 °C remained 0 % in Napa and increased from 92 % to 99 % in the SJV (c, f). Thus, the risk of heat damage is high under future climate scenarios in the SJV, but the stomatal traits have little impact on exacerbating or mitigating this risk.

modeled at the vine and not the vineyard scale. Water-saving traits would be less effective at reducing irrigation demand if slower soil moisture depletion by the vines allowed for increases in cover crop transpiration or soil evaporation. Second, the model excludes several processes that could increase vine carbon demand under future conditions. This could underestimate the constraints of the water-saving traits on ripening, especially for RCP 4.5, where A_{plant} is close to or slightly below historical levels. The model accounts for increases in leaf respiration with temperature, but not fruit, stem, or belowground respiration. Fruit and stems account for approximately 10 % and 40 % of aboveground respiration (Medrano et al., 2015; Poni et al., 2006). Warmer, wetter soil also increases root and soil microbial respiration, which can be a significant sink for plant carbon (Escalona et al., 2012; Gougoulias et al., 2014). The model is also vegetative, and does not predict fruit carbon demand. Shifting to water-saving traits made canopy water potentials ($\overline{\Psi}_{canopy}$) less negative (Fig. 7), which would increase vine water supply to the fruit and, thus, berry growth and yield (Williams et al., 2010). Increasing berry water volume would reduce sugar concentrations, which could improve quality by preventing excessive sugar accumulation, which produces bland and overly alcoholic wines (Alston et al., 2018). However, this could prevent berries from reaching adequate sugar concentrations if carbon gain is too limited. The model also assumes that vine size is constant, which is suitable for the period from veraison to harvest, when vines are managed to stop vegetative growth, but could fail to identify significant carbon limitations on canopy growth earlier in the season. Finally, the model assumes that the stomatal traits are determined only by the scion variety, while other factors, including vine age, rootstock, soil type, and temperature, can

also impact g_s (Lavoie-Lamoureux et al., 2017; Riffle et al., 2021; Soar et al., 2009). Stomatal traits can also change over time; for example, highly water-stressed vines have been shown to make stomatal closure less sensitive to water potential over the growing season (Sorek et al., 2020). Thus, some field conditions could reduce the effectiveness of water-saving plant material. Altogether, these factors could overestimate irrigation savings and underestimate carbon limitations from the water-saving traits, especially under lower CO_2 fertilization in RCP 4.5. More experimental and modeling work is needed to measure how trait and environmental changes impact vine water and carbon budgets and integrate these processes into vine- and vineyard-scale models.

Water-spending stomatal behavior has been shown to mitigate heat stress, with high stomatal conductance reducing the incidence of leaf burning for grapevines during severe heat events (Millan et al., 2023). However, our simulations predicted that mean canopy temperatures at the hottest time of day would cross thresholds for photochemical damage (40 °C) under projected average conditions in the SJV, regardless of the stomatal trait values (Greer and Weedon, 2013) (Fig. 8). Thus, growers will need plant material also selected for photochemical heat resistance or management strategies to reduce heat absorption (e.g., shadecloth, east-west row orientations, and reflective sprays, such as kaolin). More modeling work is needed to evaluate whether combining these management interventions with water-saving traits makes vine carbon gain too limiting.

5. Conclusions

Overall, our findings show that selecting grapevines for water-saving stomatal traits would reduce vine transpiration and water stress under future conditions below even historical levels, despite increasing evaporative demand. However, the stomatal traits that reduced transpiration without compromising the carbon supply for ripening varied between growing regions and climate change scenarios. Thus, breeding or engineering grapevine for a range of water-saving stomatal trait values would provide plant material tailored to different regions and reduce the risk from uncertainty around future climatic conditions. By reducing water stress, the water-saving traits could even increase yield and mitigate warming impacts on berry quality. However, several processes that are not accounted for in our modeling approach could reduce the efficacy of the water-saving traits. Accounting for growth, ripening, and belowground respiration could show that the water-saving traits are too restrictive of the carbon supply, and accounting for plasticity in stomatal behavior and water loss from the soil and cover crops could show that water savings are overestimated. More modeling and experimental work is needed to evaluate how these processes mediate the effects of the stomatal traits on vine- and vineyard-scale water and carbon fluxes.

CRediT authorship contribution statement

Rami Albasha: Methodology, Investigation, Writing – original draft, Visualization. **Megan K. Bartlett:** Conceptualization, Data curation, Investigation, Writing – original draft, Visualization.

Declaration of competing interest

The authors declare that they have no known competing financial interests or personal relationships that could have appeared to influence the work reported in this paper.

Data availability

The data needed to replicate the simulations, analyses, and figures are provided at https://github.com/MB3579/Albasha_Bartlett_AgForestMeteo_2024.

Acknowledgements

This work was supported by the UC Davis College of Agricultural and Environmental Sciences and Department of Viticulture and Enology, by generous donations from the Rossi family to the department, and by the French Research Agency (grant no. ANR-19-CE20-0024 to RA). MKB designed the study and contributed to the simulations, analyses, and manuscript preparation. RA contributed to simulations, analyses, and manuscript preparation. The authors have no conflicts of interest to declare.

Supplementary materials

Supplementary material associated with this article can be found, in the online version, at doi:10.1016/j.agrformet.2024.109892.

References

Albasha, R., Fournier, C., Pradal, C., Chelle, M., Prieto, J.A., Louarn, G., Simonneau, T., Lebon, E., 2019. HydroShoot: a functional-structural plant model for simulating hydraulic structure, gas and energy exchange dynamics of complex plant canopies under water deficit—Application to grapevine (Vitis vinifera). in silico Plants 1. https://doi.org/10.1093/insilicoplants/diz007.

Alsina, M.M., Herralde, F.D., Aranda, X., Savé, R., Biel, C., 2007. Water relations and vulnerability to embolism are not related: experiments with eight grapevine cultivars. Vitis 46, 1–6.

Alston, J.M., Fuller, K.B., Lapsley, J.T., Soleas, G., 2018. Too much of a good thing? Causes and consequences of increases in sugar content of California wine grapes. World Scientific Handbook in Financial Economics Series. World Scientific, pp. 135–163. https://doi.org/10.1142/9789813232747_0006.

Alston, J.M., Sambucci, O., 2019. Grapes in the world economy. In: Cantu, D., Walker, M. A. (Eds.), The Grape Genome, Compendium of Plant Genomes. Springer International Publishing, Cham, pp. 1–24. https://doi.org/10.1007/978-3-030-18601-2_1.

Anderson, K., Nelgen, S., 2020. Which Winegrape Varieties are Grown Where? A Global Empirical Picture. University of Adelaide Press, Adelaide, Australia.

Atlin, G.N., Cairns, J.E., Das, B., 2017. Rapid breeding and varietal replacement are critical to adaptation of cropping systems in the developing world to climate change. Glob. Food Sec. 12, 31–37. https://doi.org/10.1016/j.gfs.2017.01.008.

Bailey, B.N., Stoll, R., Pardyjak, E.R., Miller, N.E., 2016. A new three-dimensional energy balance model for complex plant canopy geometries: model development and improved validation strategies. Agric. For. Meteorol. 218–219, 146–160. https://doi.org/10.1016/j.agrformet.2015.11.021.

Bartlett, M.K., Sinclair, G., 2021. Temperature and evaporative demand drive variation in stomatal and hydraulic traits across grape cultivars. J. Exp. Bot. 72, 1995–2009. https://doi.org/10.1093/jxb/eraa577.

Burchard-Levine, V., Nieto, H., Kustas, W.P., Gao, F., Alfieri, J.G., Prueger, J.H., Hipps, L. E., Bambach-Ortiz, N., McElrone, A.J., Castro, S.J., Alsina, M.M., McKee, L.G., Zahn, E., Bou-Zeid, E., Dokoozlian, N., 2022. Application of a remote-sensing three-source energy balance model to improve evapotranspiration partitioning in vineyards. Irrig. Sci. 40, 593–608. https://doi.org/10.1007/s00271-022-00787-x.

Burgess, M.G., Ritchie, J., Shapland, J., Pielke, R., 2021. IPCC baseline scenarios have over-projected CO_2 emissions and economic growth. Environ. Res. Lett. 16, 014016 https://doi.org/10.1088/1748-9326/abcdd2.

Burnham, K.P., Anderson, D.R., 2010. Model Selection and Multimodel Inference: A Practical Information-Theoretic Approach, 2nd ed. Springer, New York, NY.

Caine, R.S., Yin, X., Sloan, J., Harrison, E.L., Mohammed, U., Fulton, T., Biswal, A.K., Dionora, J., Chater, C.C., Coe, R.A., Bandyopadhyay, A., Murchie, E.H., Swarup, R., Quick, W.P., Gray, J.E., 2019. Rice with reduced stomatal density conserves water and has improved drought tolerance under future climate conditions. New Phytol. 221, 371–384. https://doi.org/10.1111/nph.15344.

Carsel, R.F., Parrish, R.S., 1988. Developing joint probability distributions of soil water retention characteristics. Water Resour. Res. 24, 755–769. https://doi.org/10.1029/WR024i005p00755.

CDFA, 2022. California Grape Acreage Report, 2021 Summary. National Agricultural Statistics Service, Pacific Regional Office.

CDFA, 2020. California Grape Crush Report: Final 2020 [W.W.W Document]. URL. https://www.nass.usda.gov/Statistics_by_State/California/Publications/Specialty_and_Other_Releases/Grapes/Crush/Final/2020/2020_final_grape%20crush.pdf.

Chaves, M.M., Costa, J.M., Zarrouk, O., Pinheiro, C., Lopes, C.M., Pereira, J.S., 2016. Controlling stomatal aperture in semi-arid regions—the dilemma of saving water or being cool? Plant Sci. 251, 54–64. https://doi.org/10.1016/j.plantsci.2016.06.015.

Clemens, M., Faralli, M., Lagreze, J., Bontempo, L., Piazza, S., Varotto, C., Malnoy, M., Oechel, W., Rizzoli, A., Dalla Costa, L., 2022. VvEPFL9-1 knock-out via CRISPR/Cas9 reduces stomatal density in grapevine. Front. Plant Sci. 13, 878001 https://doi.org/10.3389/fpls.2022.878001.

Cochard, H., Pimont, F., Ruffault, J., Martin-StPaul, N., 2021. SurEau: a mechanistic model of plant water relations under extreme drought. Ann. For. Sci. 78, 55. https://doi.org/10.1007/s13595-021-01067-y.

Coombe, B.G., McCarthy, M.G., 2000. Dynamics of grape berry growth and physiology of ripening. Aust. J. Grape Wine Res. 6, 131–135. https://doi.org/10.1111/j.1755-0238.2000.tb00171.x.
Coupel-Ledru, A., Lebon, É., Christophe, A., Doligez, A., Cabrera-Bosquet, L., Péchier, P., Hamard, P., This, P., Simonneau, T., 2014. Genetic variation in a grapevine progeny (Vitis vinifera L. cvs Grenache×Syrah) reveals inconsistencies between maintenance of daytime leaf water potential and response of transpiration rate under drought. J. Exp. Bot. 65, 6205–6218. https://doi.org/10.1093/jxb/eru228.
Darouich, H., Ramos, T.B., Pereira, L.S., Rabino, D., Bagagiolo, G., Capello, G., Simionesei, L., Cavallo, E., Biddoccu, M., 2022. Water use and soil water balance of mediterranean vineyards under rainfed and drip irrigation management: evapotranspiration partition and soil management modelling for resource conservation. Water 14, 554. https://doi.org/10.3390/w14040554.
Dayer, S., Lamarque, L.J., Burlett, R., Bortolami, G., Delzon, S., Herrera, J.C., Cochard, H., Gambetta, G.A., 2022. Model-assisted ideotyping reveals trait syndromes to adapt viticulture to a drier climate. Plant Physiol. 190, 1673–1686. https://doi.org/10.1093/plphys/kiac361.
Deloire, A., Pellegrino, A., Rogiers, S., 2020. A few words on grapevine leaf water potential. Tech. Rev. https://doi.org/10.20870/IVES-TR.2020.3620.
Drake, J.E., Tjoelker, M.G., Vårhammar, A., Medlyn, B.E., Reich, P.B., Leigh, A., Pfautsch, S., Blackman, C.J., López, R., Aspinwall, M.J., Crous, K.Y., Duursma, R.A., Kumarathunge, D., De Kauwe, M.G., Jiang, M., Nicotra, A.B., Tissue, D.T., Choat, B., Atkin, O.K., Barton, C.V.M., 2018. Trees tolerate an extreme heatwave via sustained transpirational cooling and increased leaf thermal tolerance. Glob. Change Biol. 24, 2390–2402. https://doi.org/10.1111/gcb.14037.
Duchene, E., 2016. How can grapevine genetics contribute to the adaptation to climate change? OENO One 50. https://doi.org/10.20870/oeno-one.2016.50.3.98.
Escalona, J.M., Tomàs, M., Martorell, S., Medrano, H., Ribas-Carbo, M., Flexas, J., 2012. Carbon balance in grapevines under different soil water supply: importance of whole plant respiration: carbon balance in grapevine. Aust. J. Grape Wine Res. 18, 308–318. https://doi.org/10.1111/j.1755-0238.2012.00193.x.
Gladstone, E.A., Dokoozlian, N.K., 2003. Influence of leaf area density and trellis/training system on the light microclimate within grapevine canopies. Vitis 42, 123–131.
Goldammer, T., 2018. The Grape Grower's Handbook: A Guide to Viticulture for Wine Production, 3rd ed. Apex Publishers, Centreville, Va.
Gougoulias, C., Clark, J.M., Shaw, L.J., 2014. The role of soil microbes in the global carbon cycle: tracking the below-ground microbial processing of plant-derived carbon for manipulating carbon dynamics in agricultural systems: role of soil microbes in global carbon cycle: carbon tracking & agro-cosystem management. J. Sci. Food Agric. 94, 2362–2371. https://doi.org/10.1002/jsfa.6577.
Greer, D.H., Weedon, M.M., 2013. The impact of high temperatures on Vitis vinifera cv. Semillon grapevine performance and berry ripening. Front. Plant Sci. 4 https://doi.org/10.3389/fpls.2013.00491.
Guyot, G., Scoffoni, C., Sack, L., 2012. Combined impacts of irradiance and dehydration on leaf hydraulic conductance: insights into vulnerability and stomatal control: leaf hydraulic responses to light × dehydration. Plant Cell Environ. 35, 857–871. https://doi.org/10.1111/j.1365-3040.2011.02458.x.
Hüve, K., Bichele, I., Rasulov, B., Niinemets, Ü., 2011. When it is too hot for photosynthesis: heat-induced instability of photosynthesis in relation to respiratory burst, cell permeability changes and H2O2 formation: impaired photosynthesis under heat. Plant Cell Environ. 34, 113–126. https://doi.org/10.1111/j.1365-3040.2010.02229.x.
Jones, G.V., 2008. Climate change and the global wine industry. In: Proceedings of the Thirteenth Australian Wine Industry Technical Conference 1, p. 8.
Jones, G.V., White, M.A., Cooper, O.R., Storchmann, K., 2005. Climate change and global wine quality. Clim. Change 73, 319–343. https://doi.org/10.1007/s10584-005-4704-2.
Keller, M., Zhang, Y., Shrestha, P.M., Biondi, M., Bondada, B.R., 2015. Sugar demand of ripening grape berries leads to recycling of surplus phloem water via the xylem: phloem water recycling in grape berries. Plant Cell Environ. 38, 1048–1059. https://doi.org/10.1111/pce.12465.
Klink, K., 1999. Trends in mean monthly maximum and minimum surface wind speeds in the coterminous United States, 1961 to 1990. Clim. Res. 13, 193–205. https://doi.org/10.3354/cr013193.
Lavoie-Lamoureux, A., Sacco, D., Risse, P.-A., Lovisolo, C., 2017. Factors influencing stomatal conductance in response to water availability in grapevine: a meta-analysis. Physiol. Plant 159, 468–482. https://doi.org/10.1111/ppl.12530.
Leuning, R., 1995. A critical appraisal of a combined stomatal-photosynthesis model for C3 plants. Plant Cell Environ. 18, 339–355. https://doi.org/10.1111/j.1365-3040.1995.tb00370.x.
Levin, A.D., Williams, L.E., Matthews, M.A., 2020. A continuum of stomatal responses to water deficits among 17 wine grape cultivars (Vitis vinifera). Funct. Plant Biol. 47, 11–25. https://doi.org/10.1071/FP19073.
Martínez-Lüscher, J., Chen, C.C.L., Brillante, L., Kurtural, S.K., 2020. Mitigating heat wave and exposure damage to "Cabernet Sauvignon" wine grape with partial shading under two irrigation amounts. Front. Plant Sci. 11, 579192 https://doi.org/10.3389/fpls.2020.579192.
Martorell, S., Medrano, H., Tomàs, M., Escalona, J.M., Flexas, J., Diaz-Espejo, A., 2015. Plasticity of vulnerability to leaf hydraulic dysfunction during acclimation to drought in grapevines: an osmotic-mediated process. Physiol. Plant 153, 381–391. https://doi.org/10.1111/ppl.12253.
Medrano, H., Perez Peña, J., Prieto, J.A., Tomàs, M., Franck, N., Escalona, J.M., 2015. Carbon balance in grapevine under a changing climate. Grapevine in a Changing Environment: A Molecular and Ecophysiological Perspective. John Wiley and Sons.
Messina, C.D., Podlich, D., Dong, Z., Samples, M., Cooper, M., 2011. Yield–trait performance landscapes: from theory to application in breeding maize for drought tolerance. J. Exp. Bot. 62, 855–868. https://doi.org/10.1093/jxb/erq329.
Millan, M., Simonneau, T., Coupe-Ledru, A., Boulord, R., Christophe, A., Pallas, B., 2023. Relationships between leaf temperature, stomatal conductance and architecture: potential impact on leaf burning among a range of genotypes in grapevine: this article is published in cooperation with the 22nd GiESCO International Meeting, hosted by Cornell University in Ithaca, NY, July 17-21, 2023. OENO One 57, 345–359. https://doi.org/10.20870/oeno-one.2023.57.2.7438.
Naor, A., Bravdo, B., Gelobter, J., 1994. Gas exchange and water relations in field-grown Sauvignon blanc grapevines. Am. J. Enol. Vitic. 45, 423–428.
Park, Y.-M., 2001. Comparative water relations of two vitis vinifera cultivars, riesling and chardonnay. Korean J. Ecol. 24, 223–226.
Parker, A.K., De Cortázar-Atauri, I.G., Van Leeuwen, C., Chuine, I., 2011. General phenological model to characterise the timing of flowering and veraison of Vitis vinifera L.: grapevine flowering and veraison model. Aust. J. Grape Wine Res. 17, 206–216. https://doi.org/10.1111/j.1755-0238.2011.00140.x.
Pathak, T., Maskey, M., Dahlberg, J., Kearns, F., Bali, K., Zaccaria, D., 2018. Climate change trends and impacts on California agriculture: a detailed review. Agronomy 8, 25. https://doi.org/10.3390/agronomy8030025.
Pielke Jr, R., Burgess, M.G., Ritchie, J., 2022. Plausible 2005–2050 emissions scenarios project between 2°C and 3°C of warming by 2100. Environ. Res. Lett. 17, 024027 https://doi.org/10.1088/1748-9326/ac4ebf.
Pierce, D.W., Cayan, D.R., Maurer, E.P., Abatzoglou, J.T., Hegewisch, K.C., 2015. Improved bias correction techniques for hydrological simulations of climate change*. J. Hydrometeorol. 16, 2421–2442. https://doi.org/10.1175/JHM-D-14-0236.1.
Pierce, D.W., Cayan, D.R., Thrasher, B.L., 2014. Statistical downscaling using Localized Constructed Analogs (LOCA). J. Hydrometeorol. 15, 28.
Pierce, D.W., Kalansky, J.F., Cayan, D.R., 2018. Climate, Drought, and Sea Level Rise Scenarios for the Fourth California Climate Assessment. California's Fourth Climate Change Assessment. California Energy Commission CNRA-CEC-2018-006.
Poni, S., Palliotti, A., Bernizzoni, F., 2006. Calibration and evaluation of a STELLA software-based daily CO_2 balance model in Vitis vinifera L. JASHS 131, 273–283. https://doi.org/10.21273/JASHS.131.2.273.
Prieto, J.A., Louarn, G., Perez Peña, J., Ojeda, H., Simonneau, T., Lebon, E., 2012. A leaf gas exchange model that accounts for intra-canopy variability by considering leaf nitrogen content and local acclimation to radiation in grapevine (Vitis vinifera L.): modelling intra-canopy variability on gas exchange. Plant Cell Environ. 35, 1313–1328. https://doi.org/10.1111/j.1365-3040.2012.02491.x.
Riffle, V., Palmer, N., Casassa, L.F., Dodson Peterson, J.C., 2021. The effect of grapevine age (Vitis vinifera L. cv. Zinfandel) on phenology and gas exchange parameters over consecutive growing seasons. Plants 10, 311. https://doi.org/10.3390/plants10020311.
Romero, P., Botía, P., Gil-Muñoz, R., Del Amor, F.M., Navarro, J.M., 2023. Evaluation of the effect of water stress on clonal variations of Cv. Monastrell (Vitis vinifera L.) in South-Eastern Spain: physiology, nutrition, yield, berry, and wine-quality responses. Agronomy 13, 433. https://doi.org/10.3390/agronomy13020433.
Sadras, V.O., Montoro, A., Moran, M.A., Aphalo, P.J., 2012. Elevated temperature altered the reaction norms of stomatal conductance in field-grown grapevine. Agric. For. Meteorol. 165, 35–42. https://doi.org/10.1016/j.agrformet.2012.06.005.
Schultz, H.R., 2003. Differences in hydraulic architecture account for near-isohydric and anisohydric behaviour of two field-grown Vitis vinifera L. cultivars during drought. Plant Cell Environ. 26, 1393–1405. https://doi.org/10.1046/j.1365-3040.2003.01064.x.
Schwalm, C.R., Glendon, S., Duffy, P.B., 2020. RCP8.5 tracks cumulative CO_2 emissions. Proc. Natl. Acad. Sci. U.S.A. 117, 19656–19657. https://doi.org/10.1073/pnas.2007117117.
Sinclair, T.R., Hammer, G.L., van Oosterom, E.J., 2005. Potential yield and water-use efficiency benefits in sorghum from limited maximum transpiration rate. Funct. Plant Biol. 32, 945–952. https://doi.org/10.1071/FP05047.
Sinclair, T.R., Messina, C.D., Beatty, A., Samples, M., 2010. Assessment across the United States of the Benefits of Altered Soybean Drought Traits. Agron. J. 102, 475–482. https://doi.org/10.2134/agronj2009.0195.
Soar, C.J., Collins, M.J., Sadras, V.O., 2009. Irrigated Shiraz vines (Vitis vinifera) upregulate gas exchange and maintain berry growth in response to short spells of high maximum temperature in the field. Funct. Plant Biol. 36, 801–814. https://doi.org/10.1071/FP09101.
Sorek, Y., Grinshtein, S., Netzer, Y., Shtein, I., Jansen, S., Hochberg, U., 2020. An increase in xylem embolism resistance of grapevine leaves during the growing season is coordinated with stomatal regulation, turgor loss point, and intervessel pit membranes. New Phytol. https://doi.org/10.1111/nph.17025.
Soualiou, S., Wang, Z., Sun, W., De Reffye, P., Collins, B., Louarn, G., Song, Y., 2021. Functional–structural plant models mission in advancing crop science: opportunities and prospects. Front. Plant Sci. 12, 747142 https://doi.org/10.3389/fpls.2021.747142.
Speirs, J., Binney, A., Collins, M., Edwards, E., Loveys, B., 2013. Expression of ABA synthesis and metabolism genes under different irrigation strategies and atmospheric VPDs is associated with stomatal conductance in grapevine (Vitis vinifera L. cv Cabernet Sauvignon). J. Exp. Bot. 64, 1907–1916. https://doi.org/10.1093/jxb/ert052.
Tombesi, S., Nardini, A., Farinelli, D., Palliotti, A., 2014. Relationships between stomatal behavior, xylem vulnerability to cavitation and leaf water relations in two cultivars of *Vitis vinifera*. Physiol. Plant 152, 453–464. https://doi.org/10.1111/ppl.12180.
Tortosa, I., Escalona, J.M., Toro, G., Douthe, C., Medrano, H., 2020. Clonal behavior in response to soil water availability in tempranillo Grapevine Cv: from plant growth to

water use efficiency. Agronomy 10, 862. https://doi.org/10.3390/agronomy10060862.
van Genuchten, M.Th., 1980. A closed-form equation for predicting the hydraulic conductivity of unsaturated soils. Soil Sci. Soc. Am. J. 44, 892–898. https://doi.org/10.2136/sssaj1980.03615995004400050002x.
Van Leeuwen, C., Trégoat, O., Choné, X., Bois, B., Pernet, D., Gaudillère, J.-P., 2009. Vine water status is a key factor in grape ripening and vintage quality for red Bordeaux wine. How can it be assessed for vineyard management purposes? OENO One 43, 121. https://doi.org/10.20870/oeno-one.2009.43.3.798.
van Vuuren, D.P., Edmonds, J., Kainuma, M., Riahi, K., Thomson, A., Hibbard, K., Hurtt, G.C., Kram, T., Krey, V., Lamarque, J.-F., Masui, T., Meinshausen, M., Nakicenovic, N., Smith, S.J., Rose, S.K., 2011. The representative concentration pathways: an overview. Clim. Change 109, 5–31. https://doi.org/10.1007/s10584-011-0148-z.
Villalobos-González, L., Muñoz-Araya, M., Franck, N., Pastenes, C., 2019. Controversies in midday water potential regulation and stomatal behavior might result from the environment, genotype, and/or rootstock: evidence from Carménère and Syrah grapevine varieties. Front. Plant Sci. 10, 1522. https://doi.org/10.3389/fpls.2019.01522.
Vivin, P., Lebon, É., Dai, Z., Duchêne, E., Marguerit, E., García de Cortázar-Atauri, I., Zhu, J., Simonneau, T., Van Leeuwen, C., Delrot, S., Ollat, N., 2017. Combining ecophysiological models and genetic analysis: a promising way to dissect complex adaptive traits in grapevine. OENO One 51, 181–189. https://doi.org/10.20870/oeno-one.2016.0.0.1588.
Vivin, Ph., Castelan, M., Gaudillère, J.P., 2002. A source/sink model to simulate seasonal allocation of carbon in grapevine. Acta Hortic. 43–56. https://doi.org/10.17660/ActaHortic.2002.584.4.
Vos, J., Evers, J.B., Buck-Sorlin, G.H., Andrieu, B., Chelle, M., De Visser, P.H.B., 2010. Functional–structural plant modelling: a new versatile tool in crop science. J. Exp. Bot. 61, 2101–2115. https://doi.org/10.1093/jxb/erp345.
Waichler, S.R., Wigmosta, M.S., 2003. Development of hourly meteorological values from daily data and significance to hydrological modeling at H. J. Andrews experimental forest. J. Hydrometeor. 4, 251–263, 10.1175/1525-7541(2003)4<251:DOHMVF>2.0.CO;2.
Walker, B.J., Drewry, D.T., Slattery, R.A., VanLoocke, A., Cho, Y.B., Ort, D.R., 2018. Chlorophyll can be reduced in crop canopies with little penalty to photosynthesis. Plant Physiol. 176, 1215–1232. https://doi.org/10.1104/pp.17.01401.
Webb, L., Whiting, J., Watt, A., Hill, T., Wigg, F., Dunn, G., Needs, S., Barlow, E.W.R., 2010. Managing grapevines through severe heat: a survey of growers after the 2009 summer heatwave in South-eastern Australia. J. Wine Res. 21, 147–165. https://doi.org/10.1080/09571264.2010.530106.
White, M.A., Diffenbaugh, N.S., Jones, G.V., Pal, J.S., Giorgi, F., 2006. Extreme heat reduces and shifts United States premium wine production in the 21st century. Proc. Natl. Acad. Sci. 103, 11217–11222. https://doi.org/10.1073/pnas.0603230103.
Williams, L.E., 2014. Determination of evapotranspiration and crop coefficients for a chardonnay vineyard located in a cool climate. Am. J. Enol. Vitic. 65, 159–169. https://doi.org/10.5344/ajev.2014.12104.
Williams, L.E., Grimes, D.W., Phene, C.J., 2010. The effects of applied water at various fractions of measured evapotranspiration on reproductive growth and water productivity of Thompson Seedless grapevines. Irrig. Sci. 28, 233–243. https://doi.org/10.1007/s00271-009-0173-0.
Williams, L.E., Levin, A.D., Fidelibus, M.W., 2022. Crop coefficients (Kc) developed from canopy shaded area in California vineyards. Agric. Water Manag. 271, 107771 https://doi.org/10.1016/j.agwat.2022.107771.
Wilson, T.S., Sleeter, B.M., Cameron, D.R., 2016. Future land-use related water demand in California. Environ. Res. Lett. 11, 054018 https://doi.org/10.1088/1748-9326/11/5/054018.
Wolf, A., Anderegg, W.R.L., Pacala, S.W., 2016. Optimal stomatal behavior with competition for water and risk of hydraulic impairment. Proc. Natl. Acad. Sci. 113, E7222–E7230. https://doi.org/10.1073/pnas.1615144113.
Zaman-Allah, M., Jenkinson, D.M., Vadez, V., 2011. A conservative pattern of water use, rather than deep or profuse rooting, is critical for the terminal drought tolerance of chickpea. J. Exp. Bot. 62, 4239–4252. https://doi.org/10.1093/jxb/err139.